Materials adopted for particle beam windows in relevant experimental facilities

Review Article

Materials adopted for particle beam windows in relevant experimental facilities

Lorenzo Notari[*] and Michele Pasquali[†]
Sapienza University of Rome, Via Eudossiana 18, 00184 Rome, Italy

Federico Carra[‡] and Marcello Losasso[§]
Conseil Européen pour la Recherche Nucléaire, Esplanade des Particules 1, 1211 Geneva 23, Switzerland

Marilena Tomut[‖]
University of Münster, Schlossplatz 2, 48149 Münster, Germany
and GSI Helmholtzzentrum für Schwerionenforschung, Planckstrasse 1, 64291 Darmstadt, Germany

(Received 8 June 2023; accepted 7 December 2023; published 12 February 2024)

A beam vacuum window is a thin interface of separation between a volume under vacuum and a volume at a higher pressure traversed by particle beams. Their application is not only limited to particle accelerators, where they are typically installed inside the beamline to separate vacuum sectors, but also extends to other fields of nuclear research and to high-power hadron beam applications, such as spallation neutron sources and accelerator-driven systems. The main issue concerning the beam window technology resides intrinsically in the dual role of these components: the thickness of the window is supposed to be as thin as possible to allow the passage of the particles through matter with minimal interaction but, at the same time, enough resistant to maintain the required differential pressure between the two environments.

DOI: 10.1103/PhysRevAccelBeams.27.024801

I. INTRODUCTION

A beam vacuum window is a thin interface of separation between a volume under vacuum and a volume at higher pressure traversed by particle beams. Their application is not limited to particle accelerators, where they are typically installed inside the beamline to separate vacuum sectors but also extends to other fields of nuclear research and to high-power hadron beam applications, such as spallation neutron sources and accelerator-driven systems (ADS) [1].

The history of the beam windows is extensive but not well defined: the international standard designs have never been proposed, and each research center has independently developed very different designs based on the unique characteristics of the beam. In the past, when accelerator facilities operated at energies significantly lower than those of today, it was not infrequent to find windows constructed from common materials like steel or aluminum.

The thickness of a beam window is an important element of its use: in the case of the high thickness of the interface, the interaction with the beam increases, and with this the probability of intercepting particles that release heat inside the component. The thickness of the window is therefore supposed to be as thin as possible to allow the passage of the particles through matter with minimal interaction and beam distortion but, at the same time, enough resistant to maintain the required differential pressure between the two environments: the satisfaction of these competing demands is the main issue concerning the beam-window technology.

The research and development of innovative materials and designs capable of withstanding higher pressure loads, and more severe beam-induced thermal stresses have become extremely relevant as the energy and pulse intensities of new accelerator facilities have increased. Another critical requirement is the safe and reliable operation of future facilities as well as the prevention of failures resulting from radiation damage and the combined effect of pressure waves and thermal stresses.

An overview of the relevant characteristics that beam-window materials are required to possess for their adoption in accelerator facilities is provided in Sec. II. In the current paper, the results of an extensive bibliographical research on the materials adopted for beam-window applications are reported. Specifically, Sec. III is dedicated to the metallic

[*]notari.1692925@studenti.uniroma1.it
[†]michele.pasquali@uniroma1.it
[‡]federico.carra@cern.ch
[§]marcello.losasso@cern.ch
[‖]mtomut@uni-muenster.de

materials, while the other nonmetallic materials, the adoption of which is relatively recent for accelerator components, is covered in Sec. IV. Section V offers a quantitative comparison of the features of the materials mentioned in the previous sections through the use of figures of merit developed specifically for beam-intercepting devices, with the ambition to suggest a more targeted and faster approach in the selection process of materials for beam windows. Some conclusions from the work are discussed in Sec. VI.

A metal that exhibits excellent characteristics for beam-window applications is beryllium. The high melting point, high specific heat, and low nuclear interaction cross section are just a few causes that have led to the adoption of this metal in numerous beam-window designs. It is the best material for applications, where it is essential to minimize to the maximum extent the absorption of the particles with the matter, and for this reason, it is frequently used for windows inside x-ray tubes and accelerator beamlines.

Titanium alloys are characterized by the highest specific strength compared to any other metallic element, by the high resistance to corrosion and fatigue stresses, and by the reduced activation in harsh radiation environments. These characteristics make these alloys incredibly interesting for use in the nuclear sector and explain why this material was adopted for beam windows in many internationally renowned accelerators and high-power hadron beam applications around the world, including CERN, Fermilab, and Japan Proton Accelerator Research Complex (J-PARC).

The exceptional corrosion resistance and ultimate tensile strength of the Ni-based superalloy Inconel 718 make it a great candidate for beam windows, in particular in those facilities, in which the proper and safe operation must be ensured under critical exposure conditions to high-energy proton and neutron irradiation.

Austenitic stainless steels are frequently utilized in the construction of beam windows not only on the basis of their high corrosion resistance and ease of fabrication but also especially by virtue of the well-established knowledge of their behavior under radiation-exposed environments as a result of decades of experience in the nuclear power field. Martensitic stainless steels combine properties of good thermal conductivity and low coefficient of thermal expansion, desirable for beam windows applications, with steel-typical high mechanical strength and, above all, excellent corrosion resistance. These characteristics make these metals particularly suited to implementations, where very high-energy particle irradiation and strong corrosiveness conditions are established, as in the case of the future accelerator-driven subcritical reactors.

The excellent thermal conductivity and the radiation damage resistance of aluminum alloys have led to the use of many types of this metal in different kinds of beam windows applications, including accelerator beamlines and spallation neutron sources. Despite the relatively low melting point, the high lightness, and transparency to particle interaction make it possible to minimize the scattering of the crossing beam and to reduce strongly the amount of deposited heat, with the effect of mitigating the thermal loads and delaying the occurrence of creep deformation.

II. MAIN PROPERTIES OF BEAM-WINDOW MATERIALS

This section is intended to offer a comprehensive overview of the specific characteristics that make certain materials particularly well suited for the construction of beam windows.

A. Transparency to beam particles

The first element to consider is the effect of the particles traversing the beam window. In passing through matter, charged particles ionize or excite the atoms or molecules they encounter. This process results in a gradual loss of a portion of the beam energy (denoted as E) being transferred to the surrounding material [2]. Multiple scattering, ionization, and nuclear reactions are integral aspects of the interaction between the particle beams and vacuum window materials. Coulomb scattering, arising from electromagnetic interactions between charged particles and electric fields of atoms or nuclei in matter, along with nuclear reactions, contributes to the immediate beam losses within the traversed region of the window [3]. Naturally, the density of the window material profoundly influences the scattering process. In the case of proton beams, the probability of undergoing Rutherford scattering is proportional to the square of the atomic number of the target nuclei. Consequently, materials with lower atomic numbers have an advantage in minimizing beam loss. Otherwise, multiple scattering emerges as the primary cause of emission dilution, resulting in an increase in the beam divergence. It is a statistical process that does not modify the azimuthal symmetry of the particle on its original trajectory: if the window is thin, Coulomb multiple scattering changes the direction of the incident beam particle without altering its energy or position [4]. The understanding of such interaction mechanisms is essential for the appropriate choice of the window material and geometry as well as for a precise assessment of the beam losses.

An indication of a material's ability to slow down energetic particles traveling through its interior is called stopping power ($S = -dE/dx$). Given a specific type of particle with a certain kinetic energy and a target material, the *stopping power* is the amount of kinetic energy lost relative to the thickness of the material traveled [5]. For a particle accelerator facility designed and engineered to operate at a given energy level, the atomic number Z and the mass number A are the two main variables that can be taken into account to minimize the interaction between particles and matter.

Since the stopping power scales with Z, the high transparency to high-energy particles can be achieved only by resorting to low-Z materials. A useful parameter to determine the transparency of a beam window is given by the ratio between the thickness and the radiation length of the material [6]:

$$N = \frac{d}{X_0}, \tag{1}$$

where d is the thickness of the beam window and X_0 is the radiation length of a material, i.e., the mean length to reduce the energy of an electron by the factor $1/e$:

$$E = E_0\, e^{-x/X_0}. \tag{2}$$

Since X_0 is inversely proportional to the atomic number Z, it follows that the bigger the radiation length of a material, the more "transparent" to radiation it is.

In conclusion, the most effective approach to mitigate the effects of beam quality deterioration and energy loss arising from interaction mechanisms is to opt for lightweight materials in the construction of vacuum windows. In addition, it is crucial, when designing a beam window, to guarantee that its thickness d remains significantly smaller than one radiation length. A few examples of low-Z materials selected for beam windows are aluminum, beryllium, and graphitic materials.

B. Thermal requirements

The thermal properties of materials are another important factor to consider, as they are directly related to particle penetration into matter. As mentioned above, particles lose energy by different interaction mechanisms (ionization, multiple scattering, etc.) while passing through matter. All the energy content deposited into the matter is ultimately converted into heat.

This heat generation focused on a small portion of matter may result in a significant increase in temperature: the persistent and prolonged application of thermomechanical stresses induced by the beam to the structure can weaken the material and even lead to unexpected failure. It is precisely for this reason that the candidate materials for beam windows must have extremely high thermal conductivity (k), high specific heat capacity (c_{p}), and very low thermal expansion coefficients (CTE). If the k is too low, the heat produced by the beam passage can take too much time to propagate toward the window's edge, thereby accumulating at the center of the window that, in the worst-case scenario, may even melt. In light of this, when designing the beam window, it is essential to analytically calculate the thermal profile and verify that the highest temperature obtained is lower than the melting temperature of the material by a specific safety margin.

The thermal design of vacuum windows must consider specific beam characteristics and, especially, the power of the type of incident beams. In the case of spallation neutron sources, at least three types of time structures may be distinguished: continuous sources, short pulse sources, and long pulse sources. Most of the large-scale currently operational spallation sources employ a short-pulsed proton beam (of the order of a few μs) to produce neutrons [7]. Examples of short-pulsed high-power proton accelerators currently in operation for the major existing spallation source facilities may be found at the British Rutherford Appleton Laboratory, at the American Los Alamos National Laboratory, and at the Japan Proton Accelerator Research Complex (J-PARC). A long-pulsed source consists of a spallation source fed directly from a pulsed linear accelerator: a long proton pulse of 2.86 ms at 2 GeV is expected to be produced by the European Spallation Source (ESS) under construction at Lund, Sweden. A high value of specific heat is particularly sought after in beam windows exposed to pulsed beams, as it is directly connected to the increase in temperature of the material for a given power absorbed. The continuous spallation sources are much less widespread than pulsed ones and the only significant example of this type is provided by the Swiss Spallation Neutron Source (SINQ) at the Paul Scherrer Institut (PSI), where the continuous proton beam is sent by the PSI Ring Cyclotron. In the case of continuous beams, materials with extremely high thermal conductivity values, capable of spreading the heat continuously deposited, are even more appreciated for beam-window applications [8,9].

In the case of pulsed beams, the instantaneous temperature rise at the center of the beam distribution is undoubtedly the most critical factor in the thermal design of beam windows. A simple conservative estimation of the largest temperature increase is proposed here. Consider a window whose thickness is much less than the radiation length $d \ll X_0$ (it is, therefore, reasonable to suppose that all energy is deposited inside the target) and assume a typical round Gaussian beam with a rms width σ_{beam} for the incident particles. By neglecting the temperature dependence of the heat capacity C, the instantaneous temperature increase at the center of the beam distribution is given by the following formula [10]:

$$\Delta T_{\mathrm{inst}} = \left(\frac{dE}{\rho dx}\right)\frac{N_p}{2\pi\sigma_{\mathrm{beam}}^2 C}, \tag{3}$$

where $dE/\rho dx$ is the mass stopping power, and N_p is the number of particles passing through the window.

Another aspect related to thermal loads concerns the cooling method. The strict requirement of a thin interface makes it usually impossible to install heat exchangers to remove heat from the window's center. The predominant heat removal mechanism is the thermal diffusion from the beam spot at the center to the edge. The thermal radiation

(which varies like T^4 according to the Stefan–Boltzmann law) has a significant influence only for very high-energy incident particles and for thick windows in which heat deposition is considerable. In contrast, thermal convection is prevented on the under-vacuum side of the window. On the side kept at atmospheric pressure, the windows installed into the beam dump lines (usually with reduced beam power) are passively air-cooled in most circumstances. However, in the case of windows installed in pulsed spallation sources, the main cooling method is water cooling, and different water cooling structures have been designed to adapt to the specific beam power [11,12].

C. Resistance to pressure loads

The other fundamental issue related to beam windows concerns the maintenance of the required differential pressure between the beam line vacuum and the experimental area, which is kept under atmospheric pressure. The materials adopted for vacuum window assemblies must have high mechanical strength to withstand the repeated loads due to the beam-induced thermal stress; at the same time, these separation interfaces must provide reliable mechanical performance to handle both a static differential pressure between the vacuum and the atmosphere and occasional pressure cycling during maintenance work in which the beamline is vented [13].

A vacuum window is typically designed to be able to withstand a pressure difference ΔP of about 1 atm between its two faces. The static stress corresponding to this differential pressure depends significantly on the thickness and size of the window: in particular, stress reduces with decreasing the size and with increasing the thickness of the interface. Since the choice of the thickness of windows greatly affects their ability to withstand pressure loads, it is essential to ensure that their design meets strict mechanical safety requirements. By way of example, a design criterion for circular thin windows from the TM-1380 Fermilab guidelines is described below [14].

For circular rigid thin ($d > 75$ μm) windows fixed on the edge, as is frequently the case with stainless steel and titanium windows, the allowable stress when a uniform pressure q is distributed over the entire plate must meet the following inequality:

$$\sigma_{amm} > E\left(\frac{d}{a}\right)\left[K_3\left(\frac{y}{d}\right) + K_4\left(\frac{y}{d}\right)^2\right], \tag{4}$$

where d is the thickness of the window (in mm), a the unclamped radius (in mm), q the uniform pressure on the window (in atm), σ_{amm} the allowable stress (in atm), E the Young's modulus of the window material (in atm), ν the Poisson's ratio, y the window deflection (in mm) that can be calculated from

$$\frac{qa^4}{Ed^2} = K_1\left(\frac{y}{d}\right) + K_2\left(\frac{y}{d}\right)^3, \tag{5}$$

and K_1, K_2, K_2, K_3 the coefficients for maximum stress at the center of the window [15]:

$$K_1 = \frac{5.33}{1-\nu^2} \quad K_2 = \frac{2.6}{1-\nu^2} \quad K_3 = \frac{2}{1-\nu} \quad K_4 = 0.976. \tag{6}$$

The most stringent of the two following equations shall be used to determine the allowable stress σ_{all} for thin windows:

$$\sigma_{all} = 0.5\sigma_u \qquad \sigma_{all} = 0.9\sigma_y, \tag{7}$$

where σ_u is the ultimate tensile strength (in atm) and σ_y the yield stress (in atm).

For a selected material with known mechanical properties (E, ν, σ_y, σ_u), if the size (depending on a) is a quantity fixed by the beamline design, the minimum thickness required to withstand the static pressure load can be calculated by the previous formulas by means of an iterative procedure.

D. Leak tightness

In the design phase, low-Z materials with low thermal expansion coefficient and high thermal conductivity are usually chosen to fulfill the requirements of withstanding differential pressure loads and being transparent to particles crossing the vacuum window. An excellent choice to meet these demands is the use of carbon-carbon composites (C-C) and, more in general, carbon-based materials, whose best properties are low density, large radiation length, and low thermal expansion coefficient. On the other hand, the quite high porosity and permeability of these advanced materials prevent them from meeting the vacuum requirements since this involves an unacceptably high leak rate through their interface [16]. This example highlights an additional factor to be taken into account in the selection process of the material: high impermeability to gasses (including He that can be generated inside the matter from nuclear reactions during irradiation [17]) is absolutely essential to realize the leak-tightness condition of vacuum windows, especially when ultrahigh vacuum (UHV—pressure lower than 10^{-7} Pa) is required in the accelerator complex. An effective leak-tightness of the entire assembly cannot be separated from the choice of an adequate flange to be coupled to the window and from the appropriate welding of the different components. Before a beam window becomes operational, its vacuum performance must be ascertained through leak-detection tests, which ensure that the out-gassing rate is consistent with what is envisaged from preliminary analytical or experimental calculations.

E. Machinability and fabrication

The machinability, namely the ease in which a material can be cut or shaped with a satisfactory finish, is an important factor when choosing materials to be adopted in beam-window applications. Besides, the reduction in terms of time and costs, the ease of machining allows the production of high-precision machining components, for instance, the window-integrated cooling circuits and the multimaterial multilayer beam-window designs.

As an example, beryllium, a metal that, as will be seen, exhibits excellent characteristics for beam-window applications, presents several problems in terms of manufacturing, since it is hard and brittle and produces powder instead of chips when machined. This is the reason why special machining techniques are required to avoid cracking. Moreover, its extreme toxicity and the allergic reactions provoked in the case of inhalation exacerbate the manufacturing and handling issues.

The shape and dimensions of beam windows vary considerably depending on the specific purpose for which they are designed. Passively air-cooled windows have essential geometries and particularly thin thicknesses, whereas helium or water-cooling systems are characterized by more articulate and complex beam-window designs. In the first case, circular or rectangular flat-plate beam windows are commonly adopted: this type of design is considerably easier to fabricate and requires minimal machining operations and little need for welding for manufacturing. Moreover, the addition of precurvature to windows is under investigation in certain accelerator facilities with the aim of mitigating the stress induced by the pressure differential [13].

Another aspect to be taken into account during the design and manufacturing process of the beam windows concerns the integration of this component inside the accelerator beamline. In most cases, the beam window is securely mounted on a coupling flange that guarantees a reliable adhesion between the component and the beamline capable of satisfying the needs of leak tightness and maintaining the vacuum inside the line throughout the entire accelerator running time. In addition to the sealing via coupling vacuum flanges, usually made of steel 304 or pure titanium, other joining/sealing methods are currently considered, including TIG welding, brazing, and explosive bonding. The choice of the most optimal solution to seal the window and contain any leakage clearly depends on the pressure conditions and on the chosen design but also on the material selected for the window: it is precisely for that reason that the properties of weldability and brazability cannot be ignored in the selection process of materials for beam windows [13,18]. Finally, after the installation, the entire assembly is leak checked by a series of leak-detection tests before being put into service.

F. Lifetime and failures

Another factor to consider during the design process is the estimated lifetime of a beam window, which is mainly dependent on the effects of radiation damage and mechanical fatigue.

The influence of radiation damage on the longevity and the reliability of beam windows' constituent materials and, more generally, of the beam-intercepting devices (BIDs) of the major accelerator facilities, is considered as one of the most critical challenges for future high-energy facilities. Regardless of how transparent the window's materials are to the crossing particles, they experience significant microstructure alterations as a result of their interaction. Both primary and secondary radiations may induce a high level of atomic displacements, resulting in the formation of defect structures, such as dislocation and vacancy loops, voids, vacancy clusters, helium, and hydrogen bubbles. The window's macroscopic material properties could be drastically altered as a result of these cumulative factors, making it less ductile and more prone to failure in use.

The interaction of high-energy irradiation with a material's atomic structure gives rise to two distinct yet interconnected phenomena: radiation hardening and irradiation embrittlement. Radiation hardening primarily results from the impediment of dislocation movement by irradiation-induced defects, including vacancies, interstitials, or substitutional atoms [19]. These defects disrupt the plastic deformation process, enhancing material hardness while reducing ductility. As irradiation-induced defects can annihilate over time, defect-free channels form within the material, leading to irradiation embrittlement. Microvoids tend to nucleate at specific sites, such as intersections of these channels with grain boundaries and channel interfaces, compromising the material's structural integrity. Irradiation embrittlement is characterized by decreased elongation, reduced fracture toughness, and an elevated ductile-to-brittle transition temperature (DBTT). Therefore, while radiation hardening increases material strength, it simultaneously reduces ductility and heightens susceptibility to embrittlement [20]. The extent of these effects depends on the proton energy, fluence, and the specific material in question, emphasizing the need for precise control when using proton irradiation in particle accelerator environments and other related fields. When selecting materials for beam windows, it is crucial to determine how the mechanical properties are impacted by the high radiation environment. To this end, the mechanical properties of materials taken from components after removal from service are frequently characterized and the radiation-induced change in the main properties is quantified. The displacement per atom (dpa) and gas production are two major indices of radiation damage in irradiated materials.

The residual radiation produced by particle interaction during beam operation is an important issue for the lifetime

of vacuum windows. The nuclear activation, due to the charged particle radiation over a long period of beam exposure, involves the production of different mixes of radioactive isotopes, which undergo a series of radioactive decays until eventually a stable isotope is reached. Such radioactive nuclei, with half-lives ranging from small fractions of a second to many years, can have a dramatic effect on the residual radiation of the window. An example concerns the use of copper beam windows: activated copper produces modest quantities of cobalt-60 (usually through the reaction $^{63}\mathrm{Cu}(n,\alpha)^{60}\mathrm{Co}$), which has a long half-life and high-energy radiated daughter particles, and releases a high dose over a prolonged period [21]. If water cooling structures are present, the possible activation of the water exposed to high-energy particles must be considered and monitored carefully: the main contributors to its activity are radioactive isotopes of oxygen and nitrogen produced by activation of oxygen isotopes in the cooling water, including $^{16}\mathrm{N}$, $^{17}\mathrm{N}$, and $^{19}\mathrm{O}$ [22].

The use of a certain material for beam windows applications requires that this material has been tested under irradiation before the installation since it is essential to know in advance how and how much the mechanical properties are affected if exposed to high-energy irradiation environments. The amount of radiation-induced change in the mechanical properties of materials is frequently determined by characterizing the mechanical properties of material taken from components after removal from service in a radiation environment.

The other common cause of window failure is fatigue, a mechanical phenomenon due to the cyclic loading-induced initiation and propagation of cracks in the window's material. The fatigue can be brought about by two distinct conditions, to which correspond the kinds of mechanical and thermomechanical fatigue. The first condition is due to the cyclic variation of static pressure inside the beamline: the continuous oscillation between states of maximum stress (when the vacuum is established inside the beamline) and near-zero stresses (when the beamline is evacuated and the atmospheric pressure is restored) can weaken the vacuum sealing system and eventually determine the failure of the component. Furthermore, the cyclic deposition of energy on the window and the consequent heating and cooling cycles, concurrently with the radiation-induced material damages, may have detrimental effects on the material and speed up the onset of fatigue failures. For this reason, materials capable of maintaining sufficient mechanical properties, including adequate ductility and fracture toughness throughout the beam window lifetime, are required to minimize the risk of failure during operation.

When the heat deposited on the beam window is considerable, and the temperature is constantly high, the phenomenon of creep deformation may have detrimental effects on the mechanical properties of the material. Creep is the tendency of a material to deform when exposed to temperature, structural load, and time. The temperature range in which creep deformation can occur varies depending on the material. As a general rule, the effects of creep deformation become noticeable at about 35% of the melting point. Beam windows made of aluminum alloys, with melting points of around 600 °C, are currently adopted at working temperatures slightly above this 35% threshold and therefore continuously monitored to prevent creep failures and ensure safe operation conditions [23].

Finally, the effects of corrosion and oxidation on the beam-window material exposed to the pressure side have an important role in the lifetime of this accelerator component. For vacuum windows installed in accelerator beamlines, the material is in contact with air at atmospheric pressure and, in dry conditions, corrosive phenomena are generally unlikely to be established. Excellent performance in terms of corrosion resistance is exhibited by many materials, such as copper, titanium, and nickel alloys, and selected for this component in many particle accelerator facilities. Exposure to air can have detrimental effects in those cases in which harmful and corrosive gases, such as ozone (O_3) and nitrogen oxides (NO_x), have been produced through the activation of air that interacts with high-energy particle beams. High concentrations of these gases are particularly corrosive for beryllium, a material widely used for beam windows: a greenish copper oxide was observed for Be windows in humid and nitric acid environments, and it is considered accountable for small vacuum leaks and the initiation of beryllium contamination [13]. The oxidation of beryllium windows can be prevented by applying anticorrosion coatings of various kinds on the atmospheric side of the component: metallic (Ti, Al, Ni, and Nb) and polymeric (parylenes and epoxies, mainly used for x-ray window applications) coatings are capable of protecting Be windows and extending their operating lifetime [2,24]. In the case of beam windows inside spallation sources, the pressure side is even more exposed to the radiation of high-energy particles and neutrons, originating from the spallation target. Air is often replaced by other gases or liquids, which suppress the production of radioactive corrosive gases and are inactive and noncorrosive, such as helium. The corrosion resistance is vitally important for accelerator-driven subcritical reactors: the main candidate for the spallation target material to produce neutrons for the transmutation of long-lived nuclear wastes is the liquid lead-bismuth eutectic (LBE), an alloy with the advantage of having a melting point of about 200 °C lower than that of pure lead, but at the same time highly corrosive for the all the components of the reactor [25].

III. METALLIC BEAM WINDOWS IN EXPERIMENTAL FACILITIES

This section intends to provide an overview, as complete as possible, of materials and designs adopted for beam windows in the most important experimental facilities in the whole world.

TABLE I. Relevant nuclear, physical, and mechanical properties of beryllium. The data in this table refer to the PF-60 grade, produced by Materion [26].

	Beryllium
Atomic number	4.00
Mass number	9.00
Radiation length ($g\,cm^{-2}$)	64.91
Density ($g\,cm^{-3}$)	1.84
Thermal conductivity ($W\,m^{-1}\,K^{-1}$)	216.00
Specific heat capacity ($J\,g^{-1}\,K^{-1}$)	1.93
Volumetric CTE ($10^{-6}\,K^{-1}$)	14.50
Melting temperature (°C)	1278
Young's modulus (GPa)	303
Poisson's ratio	0.15
Tensile strength (MPa)	370

A. Beryllium

Beryllium (Be) is typically used in vacuum beam windows because of its thermal qualities and very low-Z properties: it is one of the lightest metals, with low nuclear interaction cross section, and possesses extremely high specific heat, thermal conductivity, and high melting point [26]. It has excellent mechanical properties, including high rigidity, high strength, and structural stability at high temperatures. Beryllium stands out among metals in terms of specific rigidity, i.e., the ratio of elastic modulus and density: with an elastic modulus about 50% greater than that of steel and a density 30% lower than that of aluminum, Be exhibits optimum characteristics for beam windows. It is very ductile, easily machined, and can be rolled, drawn, or extruded. It is a well-known material in the nuclear field, and it is usually utilized as the main component for neutron moderators and reflectors of nuclear plants as well as for windows of x-ray tubes, by virtue of the very low absorption of x rays.

The main issue in using beryllium is that it is toxic: if a Be window fails, it contaminates the beamline and, potentially, the entire beam enclosure, with severe consequences on clean-up costs. The effects of beryllium contamination include inhalation of Be dust, which can cause chronic beryllium disease, a chronic and sometimes fatal lung condition. Relevant properties for beam windows in Beryllium (PF-60 grade) are listed in Table I.

Five of the approximately 80 windows at Fermi National Accelerator Laboratory (FNAL) use beryllium [21]. At CERN, both the TT66 vacuum window of HiRadMat (High-Radiation to Materials) and the proton beam exit window of the CERN Neutrinos to Gran Sasso (CNGS) make use of Be as thin metallic foil applied onto C-C layers [2,27].

An example of a beryllium beam window is shown in Fig. 1: the picture represents the primary vacuum-to-air beam window of the NuMI (Neutrinos at the Main Injector)

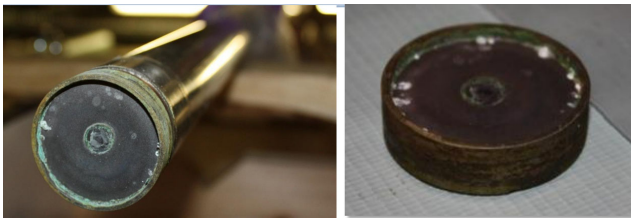

FIG. 1. NuMI beryllium beam window [13].

beamline, located at Fermilab. The PF-60 beryllium grade, manufactured by Materion, was used for the 250 μm-thick disk-shaped window in the NuMI beamline, which was operational for about 7 years, from May 2005 to April 2012. The window was exposed to proton pulsed beams with energy 120 GeV (1.57×10^{21} protons, in total) and a frequency of 0.5 Hz. The average working temperature of the component was not particularly high (around 50 °C), and a radiation damage level of approximately 0.46 dpa was assessed in the central part of the window [28]. Signs of corrosion from a humid and nitric acid environment and oxidation are prominently visible in the outer braze area and on the central beam spot. To minimize the Be oxidation at high temperatures and prevent problems caused by corrosion, a thin 0.5 μm-thick coating of titanium and niobium was applied on the atmospheric side of the Be foil of the HiRadMat vacuum window at CERN [2].

Beryllium is currently being intensively investigated for the next generation of multimegawatt high-intensity proton accelerator facilities notwithstanding the toxicity issue and the clean-up difficulties in the eventuality of a failure. In a new generation of proton accelerator-driven particle sources, such as, for instance, the Long Baseline Neutrino Facility (LBNF), a higher power version of NuMI, Be has been identified as one of the very few options for beam windows. Over the last 10 years, a large part of the research on beryllium and other promising materials for BIDs was carried out within the RaDIATE collaboration (Radiation Damage In Accelerator Target Environments), an international research partnership whose purpose is to investigate radiation damage issues in several candidate materials for application in acceleration, fission, and nuclear fusion facilities [29]. Among the activities promoted and pursued by the RaDIATE collaboration, there are new irradiation campaigns of candidate target materials, thermal shock and radiation damage investigations, and postirradiation examinations of materials recovered from dismissed beamlines [30]. For example, important findings about high-energy proton irradiation effects in beryllium come from postirradiation investigations of the aforementioned NuMI window. The investigations focused primarily on analyzing the microstructure differences between the pristine and irradiated regions of the window and on the evolution in the distribution of the main impurities (oxygen, carbon,

TABLE II. Beam parameters—Beryllium vacuum windows.

	Research center	Accel. source	Beam energy	Beam intensity		Bunch spacing
Beryllium						
TT41 CNGS proton beam window	CERN	SPS	400 GeV	1.05×10^{10} ppb	2100 bunches	5 ns
HiRadMat primary beam line window	CERN	SPS	440 GeV	1.15×10^{11} ppb	288 bunches	25 ns
NuMI target	Fermilab	Main Injector accelerator	120 GeV	4×10^{13} ppp		1.89 s

aluminum, etc.). The most pronounced effect caused by proton irradiation was the creation of transmutation products, in particular lithium, homogeneously distributed in the beryllium matrix as a solid solution, making it one of the dominant impurities of the PF-60 Be grade. In any case, this experiment does not allow predictions on the real suitability of this material for future applications, where the operating temperatures are projected to be quite higher, for instance in the range of 200–400 °C for the long-baseline neutrino facility: higher temperatures could lead to Li precipitation in the beryllium matrix (and, eventually, at grain-boundaries) but at the same time they could facilitate the ductility recovery and soften the irradiation hardening [28]. Beryllium specimens of different grades (PF-60, S-65F, S-200F, and S-200FH) have also been tested under proton irradiation at the Brookhaven Linac Isotope Producer (BLIP) facility at Brookhaven National Laboratory (BNL) in several research campaigns: good resistance against ductility loss and dimensionally stability was observed for S-200F beryllium samples for fluences up to around 1.2×10^{20} protons/cm^2 [31,32].

The most significant experiments to demonstrate the reliability of beryllium windows under beam extreme conditions, such as those expected in future high-energy multimegawatt accelerator facilities, were carried out at CERN's HiRadMat facility [33]. The high-intensity pulsed beam (4.9×10^{13} protons per 7.2 μs pulse) delivered from the CERN's Super Proton Synchrotron enables to explore the onset of failure modes (crack initiation or fracture) of different industrial grades of beryllium under controlled conditions and to identify their thermal shock limits [34]. Two types of specimens were tested inside the experimental chamber: thin disks, for deformation and crack analyses during postirradiation examinations (carried out at the Department of Materials of the University of Oxford), and slugs, for *in situ* measurements of strain and temperature, using LDVs and temperature sensors [34]. No surface cracks or failure were observed during PIEs, but is possible that there are a few microcracks on the internal part of the Be specimens (not visible with optical microscopy). The experimental results concerning the thermal shock response in terms of strain and deformation were thoroughly investigated and, in the case of beryllium grade S-200FH, numerically validated through the development of a special Johnson-Cook strength model, thus providing essential information for the design of future high-energy BIDs [35]. Nevertheless, certain critical aspects regarding the adoption of beryllium for high-energy beam windows remain unclear, particularly concerning the long-term radiation damage effects on thermal properties and structural integrity. To reduce these uncertainties and to face the challenges that increasing beam intensities impose, multiple experimental campaigns were carried out very recently and are even ongoing, including the follow-up experiment at the HiRadMat facility [36] (aimed at comparing the thermal shock response between nonirradiated Be grades and previously proton-irradiated ones) and the SMAUG (Study of beryllium MAterials Under vacuum and Glassy carbon) [37], the purpose of which is to understand the thermomechanical behavior of beryllium membranes exposed to high densities of protons. Table II presents examples of Beryllium windows installed in accelerator facilities with respective beam parameters.

B. Titanium alloys

Titanium is a transition metal well known for its properties of lightness, high strength, and good heat-transfer properties. The most valuable characteristics of this metal are the high resistance to fatigue stress and corrosion and the highest specific strength (strength-to-density ratio) of any metallic element. Moreover, its coefficient of thermal expansion has the advantage of being slightly lower than that of steel and less than half that of aluminum. In comparison with other common industrial metals, commercially pure grades of titanium have an ultimate tensile strength that is comparable to that of low-grade steel alloys but are less dense (4.5 versus 7.85 g/cm^3), while they are more than twice as strong as the most used 6061-T6 aluminum alloy, but 60% denser.

Titanium can be alloyed with iron, aluminum, vanadium, and many other elements, to produce strong, lightweight, high corrosion-resistant alloys for aerospace (jet engines, missiles, and spacecraft), nuclear (nuclear waste storage), and several other applications. The most commonly used alloy is titanium grade 5 (also known as Ti-6Al-4V), which exhibits an outstanding balance between strength, corrosion resistance, weldability, and

TABLE III. Relevant nuclear, physical, and mechanical properties of titanium alloys.

	Ti grade 2	Ti grade 5
Atomic number	21.74	20.84
Mass number	47.27	45.34
Radiation length ($g\,cm^{-2}$)	16.63	17.24
Density ($g\,cm^{-3}$)	4.51	4.43
Thermal conductivity ($W\ m^{-1}\,K^{-1}$)	16.40	6.70
Specific heat capacity ($J\,g^{-1}\,K^{-1}$)	0.52	0.53
Volumetric CTE ($10^{-6}\,K^{-1}$)	8.60	8.60
Melting temperature (°C)	1665	1632
Young's modulus (GPa)	103	113.8
Poisson's ratio	0.37	0.342
Tensile strength (MPa)	344	950

fabricability. Unlike the commercially pure (*CP*) titanium (grades 1–4), this alloy is considerably stronger, has the same stiffness and thermal properties (except for thermal conductivity, which is roughly 60% lower), and most importantly, is heat treatable.

So, in summary, this material was chosen for beam windows because of its high specific strength, good (albeit lower compared to graphitic materials and beryllium) thermal shock resistance to pulsed beams (ascribable to the relatively low Young's modulus and modest coefficient of thermal expansion), and its strong fatigue endurance limits. It is also a ductile metal and resistant to corrosion/erosion as well as a reduced activation material, an essential requirement for adoption in the nuclear field. The main drawback is the reduced thermal conductivity, which can cause problems in the diffusion of heat deposited by the intercepted particles. Relevant properties for beam windows in titanium alloys are listed in Table III.

Two grades of titanium are widely employed as beam-window materials: titanium grade 2 and titanium grade 5. The first one, an unalloyed commercially pure titanium, was used for three 100 μm-thick mobile windows of the Super Proton Synchrotron (SPS) at CERN and in a few other accelerator facilities. The Ti-6Al-4V, a high-strength dual-phase titanium alloy, on the contrary, was adopted as a beam window material in many accelerators and high-power hadron beam applications around the world, notably among them: (i) at CERN, as a single layer for two 100 μm-thick windows of TI8 transfer-line between the Super Proton Synchrotron and the Large Hadron Collider (LHC) [Fig. 2(a)] and as a thin foil applied to a C-C plate for the two windows inside the transfer-line between SPS and CNGS [Fig. 2(b)] [38]. (ii) at FNAL, where the most of the 83 beam windows are in titanium alloy [Fig. 3 [13,21]]. Figure 3(c) shows how a beam window is typically assembled: the window is first fabricated by an electron-beam process, then the foil is sandwiched between two titanium rings and, finally, the subassembly is hand-welded into a custom titanium conflat-flange. (iii) at J-PARC, where titanium alloy is adopted for the primary beam window and the target containment window of the neutrino facility [Figs. 4(a) and 4(b)] as well as for the target chamber window of the hadron facility. The primary beam window [Fig. 4(a)] comprises two 300 μm-thick partial hemispheres of titanium alloy window cooled by helium gas flowing between them.

In recent years, a collaboration between Brookhaven National Laboratory and J-PARC is underway, aiming to predict how mechanical and microstructural properties of certain titanium alloys change when exposed to high-energy proton irradiation (extremely different from that of low-energy neutrons) [40,41]. This research program, in the framework of the RaDIATE collaboration, consists of conducting high-intensity proton beam irradiation experiments on various Ti-alloy specimens at different facilities, such as HiRadMat at CERN and Brookhaven Linac Isotope Producer facility at BNL. Two principal goals were pursued: to test the mechanical properties of the titanium grade 5, currently the most widespread solution for beam windows at J-PARC and FNAL, and to understand how elemental and phase variations of titanium alloy grades affect the irradiation performance. These tests underlined

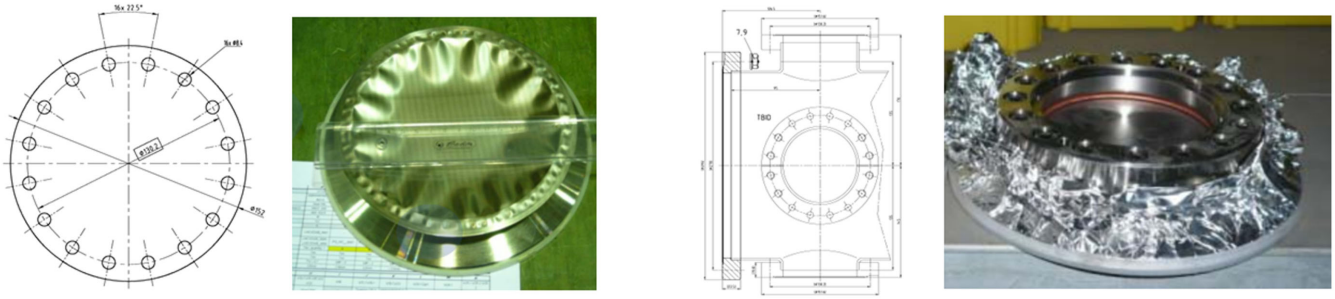

(a) (b)

FIG. 2. Technical designs and pictures of two titanium grade 5 beam windows at CERN: a target dump external beam window (a) at TI8 beamline to transfer protons and ions to the LHC and a target beam stopper external window and (b) at the beginning of the TT41 beamline for protons directed to the CERN Neutrinos to Gran Sasso (CNGS) neutrino target [16].

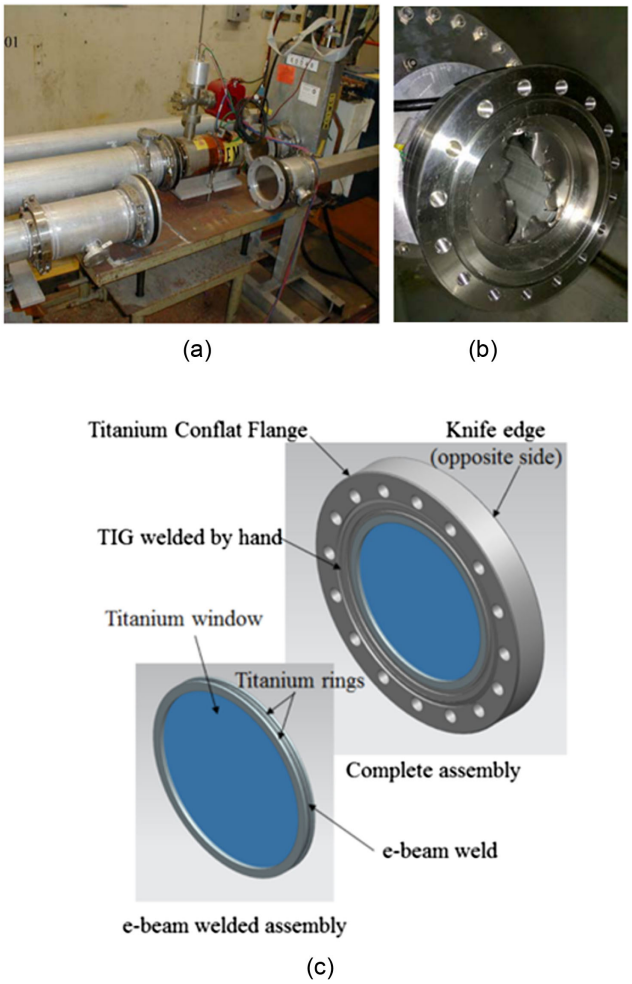

FIG. 3. Technical designs and pictures of titanium grade 5 beam windows at FNAL: an example of vacuum windows in SY120 beamline (a), an example of window failure (b) and a sketch of a typical assembly of a titanium vacuum window (c) [13].

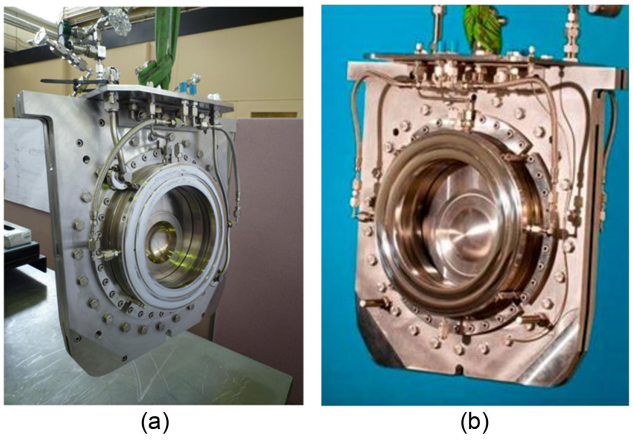

FIG. 4. Pictures of titanium grade 5 beam windows at J-PARC neutrino facility: primary beam window (a) and target containment window (b) [39,40].

that the effects of radiation damage differ significantly between the grains of α (hexagonal close packed structure) and β (body centered cubic structure) phases: high-density of defect clusters have been observed in each α-phase grain, while no visible defects have been detected for β-phase grains at low radiation doses. The high susceptibility to irradiation damage of the dual $\alpha+\beta$-phase Ti-6Al-4V is macroscopically evidenced by tensile tests' results of the high-intensity proton beam irradiation experiments conducted at the BNL BLIP facility, which shows an increase of hardness and a large decrease in ductility for fluences even lower than 0.06 dpa [41]. Likewise, high-energy proton irradiation experiments with displacement doses ranging from 0.01 to 0.3 dpa were carried out on this alloy at the Proton Irradiation Experiment facility, Paul Scherrer Institut, at temperatures around 350 °C: postirradiation microstructural observations, along with subsequent tensile testing, revealed a fine distribution of elongated precipitates, (with dimensions up to 15 μm) within the α phase. Additionally, fatigue tests were performed, demonstrating that under high-imposed strains, irradiation significantly reduced the cycle lifetime of the Ti-6Al-4V alloy [42,43]. Aside from hardening caused by the formation of dense dislocation loops in the α-phase matrix, embrittlement of the irradiation-induced ω-phase contributes to the loss of ductility of titanium grade 5. The phenomenon of ω-phase transformation in the β phase matrix is typical of titanium and zirconium alloy systems under proton beam irradiation and occurs during heat treatments of quenching and aging at temperatures below α phase formation. Basically, the embrittlement arises from the precipitation of the coarsened small-sized ω-phase particles (whose size and density tend to increase during irradiation) in the metastable β matrices, leading to a substantial decrease in ductility and an increase in material strength [41,44].

The complete understanding of α-phase hardening, ω embrittlement, and other mechanisms occurring under high-energy proton beams in titanium alloys are paramount to realize next-generation beam windows capable of maintaining enough strength and ductility even when irradiated at high doses throughout the entire operational lifetime. Current and upcoming research efforts will concentrate on enhancing the Ti-6Al-4V alloy's irradiation resistance by controlling its microstructure and implementing protective coatings. Additionally, further investigations will focus on titanium grades that are more resistant to radiation, including the ultrafine-grained Ti-6Al-4V and the metastable β-phase alloy Ti-15-333, which presents abundant nanoscale precipitates acting as sink sites to absorb irradiation defects [41,45]. These investigations will be of vital importance for the projects of future accelerator facilities in whom these alloys were chosen as a beam window material, such as the long baseline neutrino facility at FNAL, the Fermilab Proton Improvement Plan II particle accelerator for the Deep Underground

TABLE IV. Beam parameters—Ti-alloy vacuum windows.

	Research center	Proton energy	Beam intensity	Rep. rate	Cooling structure
Titanium Gr. 5					
HL-LHC beam dump window	CERN	7 TeV	2.2×10^{11} ppb 2748 bunches	25 ns	Passive cooling
Upstream window of M18 beam line, between booster and main injector	Fermilab	8 GeV	5×10^{12} ppb	0.07 s	Passive cooling
Target station T2K beam window	Tokai to Kamioka neutrino facility at J-PARC	30 GeV	3.2×10^{14} ppp	1.16 s	Double wall cooling by forced convection helium flow

Neutrino Experiment [46], under construction in South Dakota, and the International Linear Collider. Table IV presents examples of Ti-alloy windows installed in accelerator facilities with respective beam parameters.

C. Inconel 718

The nickel-based superalloys, and in particular Inconel 718 (also referred to as Alloy 718), are good candidates for beam windows applications where high strength and high corrosion resistance are primary demands for the correct and safe operation. The exceptional fatigue and creep strengths make the Inconel 718 a great choice for several structural applications in the aerospace and nuclear industries, such as jet engines, gas turbines, and fusion reactors (for example, for the jackbolts of the ITER Central Solenoid) [47]. Moreover, this alloy has a large ultimate tensile strength of roughly 0.8–1.2 GPa, excellent corrosion resistance at ambient temperature and until 500 °C and a reasonable irradiation tolerance up to a dose of 20 dpa [48]. Relevant properties for beam windows in Inconel 718 are listed in Table V

The beam window applications where Inconel 718 has been and still is utilized as a main component material are listed here: (i) The proton beam window (PBW) of the Los Alamos Neutron Science Center (LANSCE), New Mexico, USA. (ii) The PBW of the target station 1 (TS1) of ISIS Neutron and Muon Source at the Rutherford Appleton Laboratory, United Kingdom. (iii) The beam window of the Isotope Production Facility (IPF) at LANSCE. The beam assembly and the IPF testing apparatus are shown in Fig. 5. (iv) The first generation of the PBW of the Spallation Neutron Source (SNS) at Oak Ridge National Laboratory (ORNL), Tennessee, USA. The design of this proton beam window in Inconel 718 (recently replaced with a second generation PBW in aluminum alloy Al-6061-T651) is shown in Fig. 6: it consisted of two curved walls in Inconel 718 with a separation gap of 1.5 mm, in which heat deposited during irradiation was removed by cooling water flow [18].

TABLE V. Relevant nuclear, physical, and mechanical properties of Inconel 718.

	Inconel 718
Atomic number	27.04
Mass number	57.68
Radiation length ($g\,cm^{-2}$)	13.59
Density ($g\,cm^{-3}$)	8.19
Thermal conductivity ($W\,m^{-1}\,K^{-1}$)	11.40
Specific heat capacity ($J\,g^{-1}\,K^{-1}$)	0.44
Volumetric CTE ($10^{-6}\,K^{-1}$)	13.00
Melting temperature (°C)	1298
Young's modulus (GPa)	205
Poisson's ratio	0.29
Tensile strength (MPa)	1375

Much of the knowledge gained so far concerning the radiation-induced degradation in mechanical properties of this superalloy comes from the characterization tests carried out on the just mentioned beam windows after removal from service. Moreover, the tensile properties of this precipitation hardenable alloy, whose microscopic structure is fairly complex, are strongly affected not only by the proton (or other particles) irradiation but also by the different temperatures and times of the heat treatments. It is therefore important to briefly report the characteristics and differences of the two production solutions most

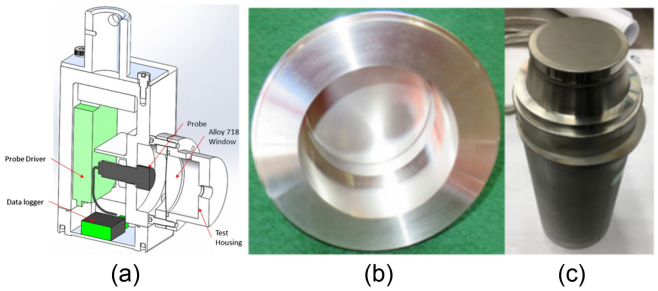

FIG. 5. (a) Computer-aided program (CAD) drawing of the IPF testing apparatus used to measure beam window deformation under different loading conditions. (b) IPF beam window and weld flange and (c) full beam window assembly [49].

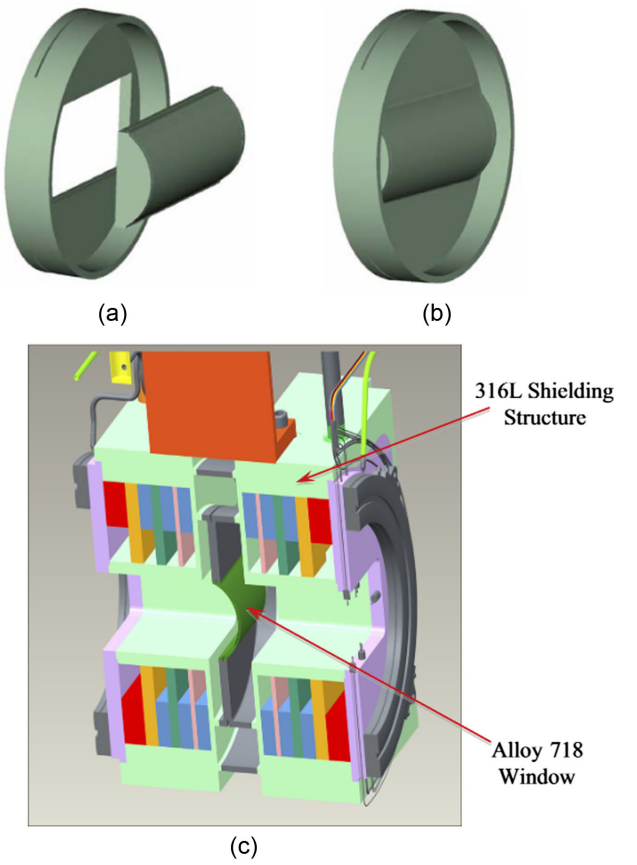

FIG. 6. First generation curved dual-wall Inconel 718 PBW at the Spallation Neutron Source: (a) Inconel 718 window and frame, (b) complete window, and (c) cross-sectional view of complete PBW assembly [18].

used for beam windows applications, such as the solution-annealed (SA) and precipitation-hardened (PH) conditions: (i) Precipitation-hardened condition: This condition is achieved by introducing a fine dispersion of γ' [$Ni_3(Al, Ti)$] and γ'' (Ni_3Nb) phases in a composite structure of the austenitic matrix and by undergoing the alloy to multistep heat treatments of aging with the purpose of increasing the strength. While the γ' phase, with a face-centered cubic (fcc) structure, is quite stable, the semicoherent body-centered-tetragonal γ'' phase is metastable and tends to transform to ordered orthorhombic δ (Ni_3Nb) phase for temperatures higher than 850 °C. (ii) Solution annealing condition: In this case, a single-phase austenitic microstructure is not strengthened by precipitation of γ' and γ'' phases and only the δ phase can be present if solution annealing is conducted at a temperature below the 1020 °C.

Inconel 718 in both PH and SA conditions was utilized for the construction of beam windows. Although the postirradiation examinations that have been carried out over the last 20 years have led to a deeper understanding of the effects of the radiation-induced damage, even today the influence of irradiation on the mechanical properties and the microstructure of this superalloy is not utterly unambiguous [50]. The differences in operational performance and degradation of mechanical properties observed for the Inconel 718 beam windows (in the SA and PH conditions) are summarized here: (i) The PH Inconel 718 proton beam window at LANSCE was removed from operation because it was leaking coolant. The tensile tests detected significant radiation-induced embrittlement during service and a decrease of the total elongation to 5% at 10 dpa and to 0% at 20 dpa [51]. (ii) The SA Inconel 718 proton beam window of the ISIS TS1 was successfully in use for almost 25 years and was removed from operation after having received a dose of 30–40 dpa upon reaching the administrative maximum dose limit (not for reasons of structural embrittlement). (iii) In light of the results of embrittlement of the PH PBW at LANSCE, solution-annealed Inconel 718 was chosen for the first generation of PBW of the Spallation Neutron Source. The service lifetime was determined by the administrative dose limit and the window was replaced after 2 years of high-energy proton irradiation, corresponding to a peak dose of 9.7 dpa, without having caused any problem with the operation of the SNS facility [50].

In conclusion, Inconel 718 in precipitation-hardened condition has been demonstrated to be more susceptible to radiation-induced changes in structure, composition, and cohesion with the matrix than the solution-annealed alloy under irradiation of neutrons, protons, and ions [47,48,52]. The mechanical behavior of PH Inconel 718 is primarily influenced by the dissolution of the γ' and γ'' phases, not stable under low-temperature irradiation. The γ'' phase, the main responsible for the hardening of the alloy, disappears even at relatively low doses (0.7 dpa). A series of recent experiments conducted on the IPF beam window at LANSCE has proved that the γ' and γ'' phases are no longer observable after irradiation to 11.3 dpa but still appreciable ductility and work-hardening capacity has remained after irradiation [52]. The last tensile tests conducted at the Swiss Spallation Neutron Source and at IPF on SA Inconel 718 samples concur that remarkable ductility is retained by the superalloy after irradiation, even at high doses, and that uniform elongation values increase from approximately 8% at 7.8 dpa to roughly 14% at 18.4 dpa [53]. However, the biggest impact on the mechanical behavior is that of the exposure of the alloy to elevated temperatures during fabrication, irradiation, or handling stages: it has been observed that postirradiation annealing at temperatures ranging from 300 and 500 °C is responsible for inducing recombination and annihilation of radiation-induced defect structures and thus alleviating hardening [48]. The large influence of thermal processes and processing conditions on the radiation-induced microstructural changes in Inconel 718 was investigated in a recent experimental campaign at the University of Michigan, where samples in SA condition were tested under 2 MeV proton ion irradiation at 360 °C [54].

TABLE VI. Beam parameters—Inconel 718 proton beam windows.

	Research center	Beam power	Proton energy	Beam intensity	Rep. rate	Cooling structure
Inconel 718						
SNS PBW (1 gen)	Oak Ridge National Laboratory	1.4 MW	1 GeV	1.5×10^{14} ppp	60 Hz	Curved dual-wall window, cooled by deionized water
ISIS Target Station 1	Rutherford Appleton Laboratory	0.2 MW	0.8 GeV	1.25×10^{15} proton per second	50 Hz	Water-cooled double window
Isotope Production Facility PBW	Los Alamos Neutron Science Center	25 kW	0.1 GeV		100 Hz	Water-cooled on target chamber side

Different thermal treatments, including solution annealing, cold work, and aging, were applied to each sample at various temperatures. The outcomes of the postirradiation investigations proved a better irradiation behavior in the high-temperature SA sample (1093 °C) compared to the low-temperature SA sample (945 °C) since a larger presence of voids and greater dislocation loop density were observed in the latter sample [54]. Table VI presents examples of Inconel 718 PBWs installed in spallation sources with respective beam parameters.

D. Stainless steels

1. Austenitic stainless steels

Austenitic steels are nonmagnetic stainless steels with high chromium and nickel content and low levels of carbon. Austenitic steels, the most popular type of stainless steel, are renowned for their formability and corrosion resistance. Unlike the body-centered cubic crystalline structure of the ferritic steels, austenitic steels have predominantly a face-centered cubic (fcc) grain structure that prevents them from being hardenable by heat treatment. This fcc grain structure is achieved by adding a sufficient quantity of austenite-stabilizing elements, such as Ni, Mn, and N, in a standard 18% chromium alloy.

The most popular grades of austenitic steels utilized for beam-windows components are AISI 304L and AISI 316L.

TABLE VII. Relevant nuclear, physical, and mechanical properties of two types of austenitic stainless steels.

	AISI 304	AISI 316
Atomic number	25.50	25.80
Mass number	54.71	55.40
Radiation length ($g\,cm^{-2}$)	14.36	14.23
Density ($g\,cm^{-3}$)	8.00	8.00
Thermal conductivity ($W\,m^{-1}\,K^{-1}$)	15.15	14.95
Specific heat capacity ($J\,g^{-1}\,K^{-1}$)	0.50	0.50
Volumetric CTE ($10^{-6}\,K^{-1}$)	17.30	17.20
Melting temperature (°C)	1425	1388
Young's modulus (GPa)	197	193
Poisson's ratio	0.15	0.15
Tensile strength (MPa)	564	560

Both are part of the 300 series, a subgroup of chromium-nickel alloys that achieve their austenitic microstructure almost exclusively by nickel alloying. The reference nomenclature for stainless steel grades is the American Standard AISI (American Iron and Steel Institute). The 304 grade, the most common of the stainless steels, typically contains 18% chromium (minimum percentage of Cr needed to completely convert all the ferrite to austenite) and 8% nickel. The production of the 316 grade provides for the addition of about 2% of molybdenum to increase corrosion resistance. The carbon content for austenitic stainless steels, which must not exceed 0.08% for straight grades, can be reduced to produce steels less susceptible to intergranular corrosion. Since the mechanical effects due to carbide precipitations are a concern for irradiated components, low carbon grades (indicated by the letter "L"), with a maximum carbon content of 0.03%, are more suitable for beam windows applications.

These steel grades offer excellent performances in terms of corrosion resistance, ease of fabrication, and welding and have good high-temperature properties. The main advantage of their use lies in the fact that their behavior after long exposure to radiation environment is well known and proven: austenitic steels are the typical choice for the cylindrical shell of the reactor pressure vessel in nuclear power plants, one of the most critical components for nuclear plants on which depends the lifetime of the reactor. Relevant properties for beam windows in austenitic stainless steels are listed in Table VII.

Numerous research centers and experimental reactors, such as the High Flux Isotope Reactor (HFIR) at ORNL and the Experimental Breeder Reactor-II (EBR-II) at Argonne National Laboratory, deal with the effects of radiation damage on these structural steels and several studies have been conducted about austenitic steels under irradiation of different types of particles at different energy levels [55]. The most life-limiting factors in the application of these stainless steels concern the precipitation of phases, the formation of cavities with the volumetric expansion of the material (the so-called void swelling), and the irradiation creep. Furthermore, numerous experimental campaigns were conducted to investigate the mechanical

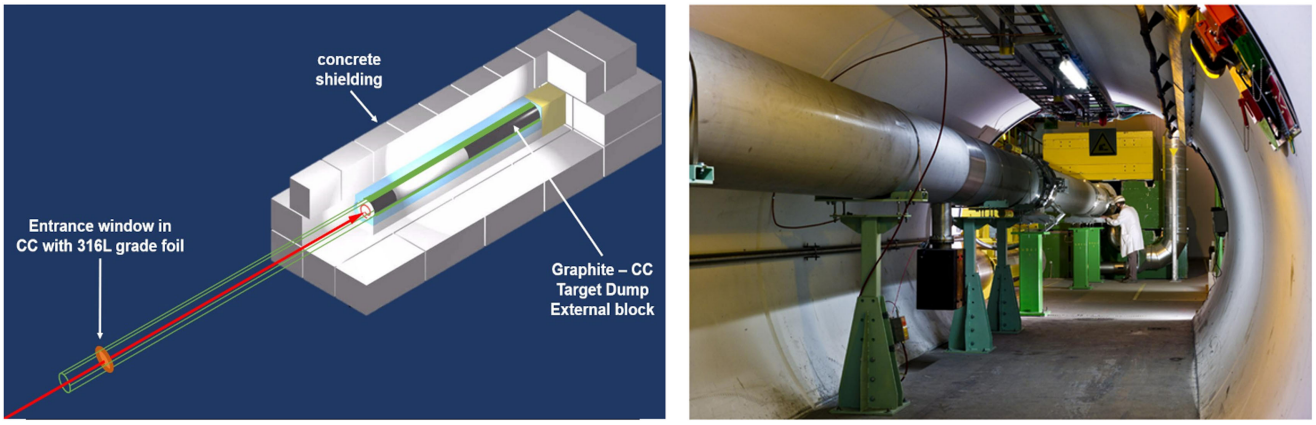

FIG. 7. (a) Sketch and (b) picture of the LHC dump block and surrounding shielding, showing the location of the entrance window [61].

degradation of these austenitic steels in high-energy proton and neutron radiation environments, aiming to evaluate their suitability as spallation source target materials. Tensile tests performed on 304L and 316L specimens exposed to 800 MeV proton beams at LANSCE have uncovered a marked reduction in ductility and radiation hardening. These findings are consistent with the databases for materials irradiated in fission reactors, with the notable exception of more pronounced radiation strengthening at higher doses, likely attributable to increased gas content [56]. The decline in ductility within the austenitic alloys is ascribed to strain localization during deformation [56]. Moreover, postirradiation investigations at LANSCE have shown that raising the test temperature from 20 to 160 °C results in a reduction in uniform elongation, specifically for measured doses between 1 and 3 dpa [57]. Recent research activities have prominently concentrated on 316LN, a nitrogen-enriched variant of 316L. This material exhibits a higher tolerance to radiation damage, maintaining good postirradiation fracture toughness and preserving a modest degree of ductility even at doses exceeding 10 dpa under spallation conditions. Consequently, this steel grade has emerged as an appealing choice for innovative beam window and target applications [58,59].

The AISI 304L (S or X5CrNi18-10, according to the EN designation) was used as the main component for nearly the totality of the beam windows installed along the beamlines of the Super Proton Synchrotron at CERN. On the other hand, the AISI 316L (or X5CrNiMo17-12-2) has been chosen for the windows of many other CERN facilities, among which the Proton Synchrotron (PS), the PS Booster, and ISOLDE. Table VIII presents examples of AISI 316L beam windows installed at CERN with respective beam parameters.

Moreover, it is important to point out that stainless steel has been selected for the entrance window of the LHC beam dump, the design of which provides for the application of a 200 μm-thick 316L grade foil on a 1.5 cm-thick C-C plate in Sigrabond 1501G. This design solution proves that this metal was considered highly reliable for withstanding the repeated dynamic thermal loads that occur when the ultimate intensity LHC beam (4.77×10^{14} protons at 7 TeV) is dumped [60]. Figures 7 and 8 show CAD drawings and pictures of the double-layer beam windows and of the LHC dump cavern. At the end of 2021, this beam window was replaced by a beam window of new conception to cope with beams of even more increasing intensity, such as the ones of the LHC Run 3 and the future High-Luminosity LHC project. This new design provides for a 1 mm-thick titanium grade 5 sheet sandwiched between two layers of 15 mm-thick C-C plates and a 10 mm-thick titanium grade 23 plate installed downstream (Fig. 9).

This beam window conception increases the reliability and robustness of this critical system to the differential

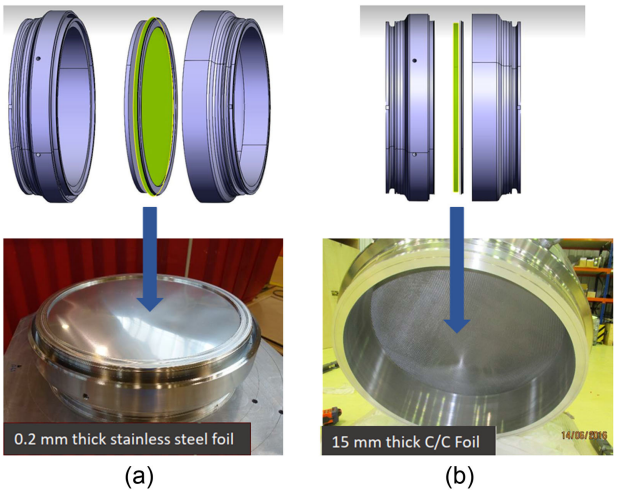

FIG. 8. CAD drawings and pictures of the entrance window, showing: (a) the 200 μm-thick stainless steel foil and (b) the 15 mm-thick C-C plate [62].

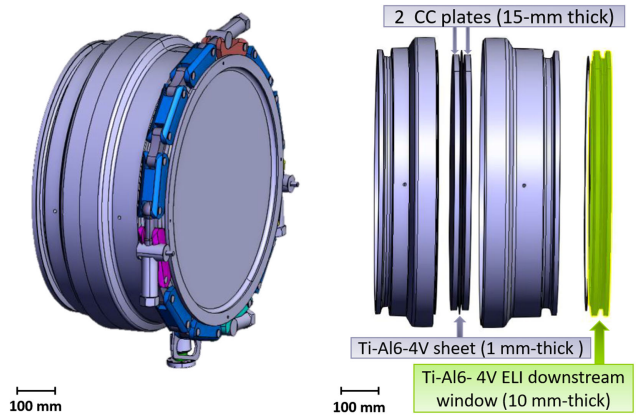

FIG. 9. CAD drawings of the new conception of the entrance window for the beam dump of LHC Run 3 and, in the future, of HL-LHC at CERN [62].

pressure and beam-induced thermal loads and is fully compatible with the future HL-LHC parameters [62].

2. Martensitic stainless steels

Martensitic stainless steels represent one of the four main varieties of stainless steels (ferritic, austenitic, duplex, and martensitic). Such steels are characterized by high strength and hardness as well as by excellent resistance to wear and corrosion. They are ferromagnetic and, differently from austenitic and ferritic stainless steels, can be hardened and tempered through aging and heat treatments. They also possess a high value of Young's modulus, a low coefficient of thermal expansion, and a high-thermal conductivity coefficient, making them excellent for heat-transfer applications.

Martensitic stainless is distinguished by its particular crystal structure. Martensitic structures are obtained through a rapid cooling (called quenching) that has the aim of "freezing" a phase that is stable at high temperatures but unstable at room temperature. After quenching, the face-centered cubic (fcc) austenite transforms into the so-called martensite, a crystalline structure with a body-centered tetragonal form. This microscopic change in the structure induces the formation of a large number of dislocations, which are responsible for the strengthening mechanism of the steel.

Given the characteristics listed above, the martensitic steels are good candidates for beam window applications in which the preservation of mechanical properties at high temperatures and decent resistance to radiation-induced embrittlement are required, such as spallation neutron source facilities and accelerator-driven subcritical reactors. Two martensitic stainless steels which provide excellent choices for beam window applications are DIN 1.4926 and T91.

The martensitic steel DIN 1.4926 (11% Cr) was used for a double-wall window in the LANSCE facility at the Los Alamos National Laboratory. The beam window, designed and realized by the Paul Scherrer Institut at Villigen (Switzerland), was irradiated with 800 MeV protons at LANSCE and, finally, investigated at Forschungszentrum Jülich (FZJ), in Germany [63]. The results obtained from this joint study between the three research centers showed that the tensile properties and the microstructure of DIN 1.4926 were considerably changed after irradiation, even at low levels of fluence (0.3 dpa). The proton irradiation experiment was conducted with the temperature maintained low, below 230 °C, in order to ascertain that the effects of embrittlement, typical of ferritic/martensitic steels at low irradiation temperatures, were observable even for the steel DIN 1.4926 [64]. The yield stress and ultimate tensile strength were observed to increase as a function of dose, leading to a progressive increase in radiation-induced hardening with fluence up to 6.8 dpa (the maximum attained dose). Moreover, the 800 MeV proton irradiation affected significantly the uniform and total elongation: the uniform elongation is strongly reduced from about 11% for pristine steel to less than 1.5% for irradiated steel. Finally, small defect clusters were observed in all the samples of the irradiated martensitic steel: their size and density increase progressively with fluence [63,65]. The martensitic stainless steel T91 (Mod. 9Cr-1Mo) is a suitable material for those beam window applications, in which high mechanical strength (larger than those of austenitic steels) and excellent corrosion resistance are required, such as in the case of the beam window of the future ADS spallation targets. T91 steel was developed by the ORNL in the 1970s. It has good thermal conductivity and a low coefficient of thermal expansion, like the other martensitic steels, but stands out for its strong corrosion resistance and good creep rupture strength. It is, therefore, an ideal material for realizing steam chambers and superheaters for boilers of power plants. Relevant properties for beam windows in martensitic stainless steels are listed in Table IX.

Different projects involve the use of this steel for the proton beam window of an accelerator-driven system,

TABLE VIII. Beam parameters—AISI 316L vacuum windows.

	Research center	Proton energy	Beam intensity	Rep. rate	Cooling structure
AISI 316					
Window at the end of the beamline from PSB to ISOLDE	CERN	1.4 Gev	3.7×10^{13} ppp		Passive cooling
LHC beam dump entrance window	CERN	7 TeV	4.77×10^{14} ppp	25 ns	Passive cooling

TABLE IX. Relevant nuclear, physical, and mechanical properties of two types of martensitic stainless steels.

	DIN 1.4924	T91
Atomic number	25.59	25.67
Mass number	55.03	55.21
Radiation length ($g\,cm^{-2}$)	14.35	14.31
Density ($g\,cm^{-3}$)	7.85	7.77
Thermal conductivity ($W\,m^{-1}\,K^{-1}$)	24.00	27.00
Specific heat capacity ($J\,g^{-1}\,K^{-1}$)	0.44	0.46
Volumetric CTE ($10^{-6}\,K^{-1}$)	10.50	11.30
Melting temperature (°C)	1425	1450
Young's modulus (GPa)	217	207
Poisson's ratio	0.28	0.3
Tensile strength (MPa)	767	585

including the MEGAwatt PIlot Experiment (MEGAPIE) at PSI and the ADS proposed by the Japan Atomic Energy Agency (JAEA) [25,66]. An accelerator-driven subcritical reactor is a hybrid system of a high-energy proton accelerator and a substantially subcritical nuclear reactor core. These promising devices could be useful to develop thorium-based energy production or to transmute high-level nuclear waste, such as minor actinides. The beam window forms the boundary component between the accelerator and the spallation target region. In this region, a liquid metal, such as lead or lead-bismuth eutectic (LBE) flows upward from the bottom of the core while being heated by the proton beam.

The ADS beam window must be able to withstand many extreme conditions at the same time, including any of the following: (i) The corrosion induced by the passage of the LBE coolant. (ii) The differential pressure between the core, in which LBE flows, and the accelerator region, kept under vacuum. The heat generation by the proton beam. (iii) The irradiation damage by neutrons and protons.

This martensitic steel was considered suitable for this purpose since it has a mechanical strength higher than those of austenitic stainless steels and it is less susceptible to corrosion damage than other materials.

MEGAPIE is an initiative launched by the French Atomic Energy Commission (CEA), the Paul Scherrer Institut (PSI), and the German Forschungszentrum Karlsruhe (FZK), to demonstrate the feasibility of a liquid LBE target for ADS spallation facilities at a beam power level of 1 MW. Figure 10(a) shows the design of the MEGAPIE target assembly with the lower liquid container and the beam window made of steel T91 [25,67]. The irradiation experiment of the MEGAPIE target took place at the SINQ facility of PSI from August to December 2006.

Experimental measurements and postirradiation examinations have provided insights into the behavior of steel T91 under fluxes of high-energy protons and spallation neutrons and in contact with flowing LBE. There are many possible causes of damage to this component, including liquid metal and irradiation embrittlement, erosion, and cyclical loads or thermal stresses. Despite the high-energy fluxes of protons and spallation neutrons, the corrosive effect of flowing LBE is not especially relevant at relatively low temperatures ($< 350\,°C$) and does not constitute a limiting factor for the lifetime of the window [69,70]. On the contrary, radiation-induced embrittlement and hardening are typical behaviors of martensitic steels at low-temperature irradiation regime, which may increase the risk of sudden brittle failure of the window: tensile tests on specimens extracted from the T91 PBW have revealed good ductility of this steel grade

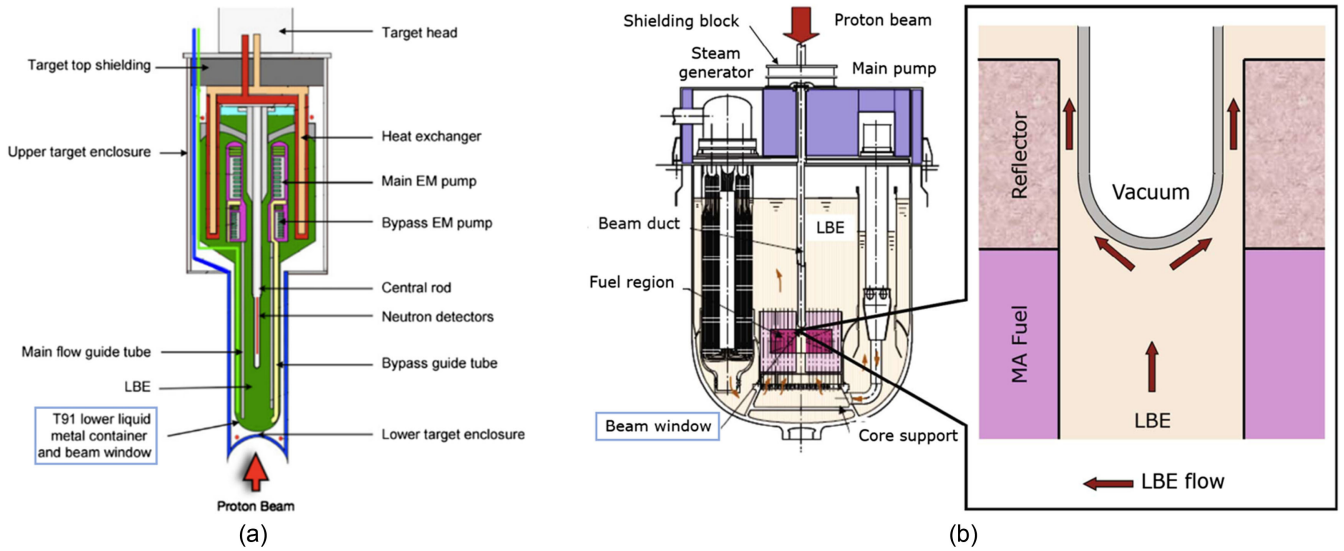

FIG. 10. (a) Schematic view of the MEGAPIE target assembly with the T91 window and the other main components indicated [67]. (b) Schematic view of the design of the LBE cooled ADS and its beam window proposed by the JAEA [68].

TABLE X. Proton beam parameters of PBWs of accelerator driven systems.

	Research center	Beam power	Proton energy	Average current	Beam intensity	Rep. rate	Cooling structure
Steel T91							
MEGAPIE PBW	SINQ target location at PSI	750 kW	0.1 GeV	1.3 mA	Continuous beam		Hemispherical window, LBE-cooled
AISI 316							
TEF-T PBW	J-PARC	250 kW	0.4 GeV	0.625 mA	3.9×10^{15} proton per second	25 HZ	Ellipse shape window, LBE-cooled

after irradiation at 6–7 dpa [69]. In addition, a series of impact Charpy tests were performed to assess the change in the ductile-to-brittle transition temperature: the outcomes proved that a dose of almost 9 dpa is necessary to produce a large shift in DBTT from the unirradiated original value (−50 °C) to the lowest operating temperature in beam-off conditions (230 °C) [71]. Such results confirm the potential of this steel grade for future ADS beam windows.

An ambitious ADS project proposed by the Japan Atomic Energy Agency consists of a high-intensity proton accelerator with 1.5 GeV beam energy, a liquid lead-bismuth eutectic spallation target, and a subcritical core ($k_{\mathrm{eff}} = 0.97$) with 800 MW thermal power. The project of the T91 beam window is one of the critical issues for the realization of the ADS, and different types of window design were suggested over the years, such as the ellipse shape and the hemispherical shape [in Fig. 10(b)], to address the problems of creep deformation, corrosion, and thermal stress caused by the proton beam [66,68]. JAEA intends to construct a Transmutation Physics Test Facility (TEF-T) within the context of the J-PARC project in order to acquire the data essential for ADS design [72]. The low-power proton pulsed beams coming from the 400 MeV LINAC of J-PARC will give the possibility to conduct irradiation tests on structural materials and engineering experiments for Pb-Bi applications aimed at determining the lifetime of the future components, including the target beam window, that will be produced in AISI 316 stainless steel in this early stage [73,74]. Table X presents the beam parameters of the above-mentioned ADS proton beam windows.

E. Aluminum alloys

Aluminum is a very interesting material for ultrahigh vacuum systems for accelerators and, in particular, for beam window applications. It is a very light material ($\rho \approx 2.7$ g cm^{-3}), with a density 2–3 times lower than that of steels or nickel alloys.

The high transparency to radiation is an excellent quality of aluminum alloys: the particles, while crossing the material, have less interaction with the matter and deposit a lower amount of heat, resulting in a smaller peak of temperature. Since the relatively low melting point is among the main defects of this material, the maximum temperature reached during irradiation is a factor that always has to be taken into account.

Moreover, the property of high transparency ensures a reduction of the residual radioactivity after machine shutdown and increased efficiency in the particle transfer: for instance, the replacement of the Inconel 718 SNS PBW with an aluminum one has caused an approximately 3%–5% increase in neutron production by the spallation target from the decreased scattering of protons having passed through the window [18].

TABLE XI. Relevant nuclear, physical, and mechanical properties of four types of aluminum alloys.

	Al-5052	$AlMg_3$	Al-5083	Al-6061
Atomic number	13.03	13.07	13.04	13.09
Mass number	27.04	27.10	27.06	27.17
Radiation length (g cm^{-2})	24.20	24.15	24.19	24.14
Density (g cm^{-3})	2.68	2.70	2.66	2.70
Thermal conductivity (W m^{-1} K^{-1})	138.00	130.00	119.70	167.00
Specific heat capacity (J g^{-1} K^{-1})	0.88	0.90	0.90	0.90
Volumetric CTE (10^{-6} K^{-1})	23.80	24.00	24.20	23.60
Melting temperature (°C)	628	617	570	617
Young's modulus (GPa)	70	68	70.3	68.9
Poisson's ratio	0.33	0.33	0.32	0.33
Tensile strength (MPa)	330	330	285.8	310

Other characteristic properties are the high thermal conductivity, the resistance to embrittlement induced by radiations, and the possibility of being easily shaped into complicated profiles by extrusion and drawing [75].

Aluminum alloys are classified into eight groups or series, according to their main alloy element. The aluminum alloys most frequently utilized for beam windows applications in radiation environments fall into two general alloy groups: the 5000-series (Al-Mg alloys) and the 6000-series (Al-Mg-Si alloys). Relevant properties for beam windows in alluminum alloys are listed in Table XI.

1. Aluminum 5000-series alloys

The Al-Mg alloys are solid-solution strengthened alloys with superb corrosion resistance in flowing water and good formability. They are used in a wide variety of industrial sectors and for marine and naval applications. Because of their high thermal conductivity and, most importantly, the excellent radiation-induced damage resistance, Al-Mg alloys are also very common in the nuclear field, for applications where an aluminum alloy with resistance qualities halfway between those of the softer 1000-series alloys (pure aluminum) and those of stronger precipitation-hardened (PH) 6000-series alloys are required.

Within this category of aluminum alloys, three specific grades were chosen for their application in beam-window applications: Al-5052, $AlMg_3$ (close to Al-5454), and Al-5083.

The Al-5052 is an aluminum alloy principally alloyed with magnesium (roughly 2.5% by weight) and chromium (0.25%). This grade, in the temper state Al-5052-H19 (where H indicates that its strength was increased by strain hardening and 19 specifies the approximate amount of cold work) was utilized for three beam windows at CERN, inside the Transfer Tunnel 20 (TT20) that connects the CERN Super Proton Synchrotron with Targets T2 (TT23 line) and T4 (TT24 line), located in the CERN North Area [38].

The aluminum-magnesium alloy $AlMg_3$, with the composition of Mg (2.72% by weight), Si (0.3%), Fe (0.25%), and Mn (0.35%), was used as the material for the safety hull of the SINQ Target-3 and irradiated in 1998 and 1999. In Fig. 11, the design of the safety hull is illustrated schematically. The safety hull is a double-walled container of about 20 cm in diameter and 2 m long, where the lower part acts as an entrance window for the proton beam coming up from the vacuum region below. Heavy water (D_2O) flows in the gap between the two walls to cool the hull and the target block during irradiation [76].

The aluminum alloy most widely used for PBWs of spallation neutron sources is the Al-5083. This alloy, composed of magnesium (about 4.5% in wt) with traces of manganese and chromium, features high corrosion resistance to water, and an exceptional strength after welding, to the point of being unrivalled in terms of strength among the

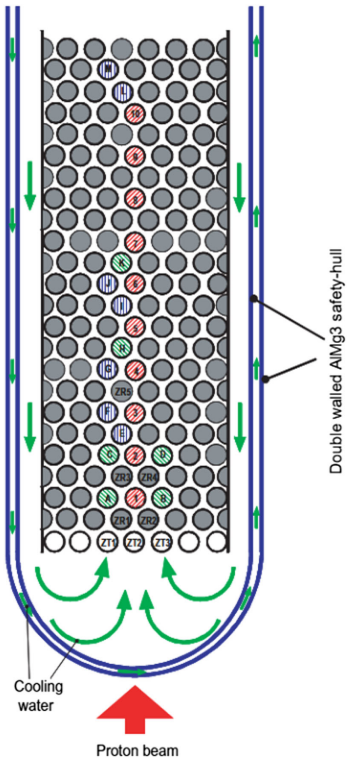

FIG. 11. A schematic sketch of the lower part of SINQ Target-3 $AlMg_3$ safety-hull [76].

nonheat treatable aluminum alloys. It is always subjected to homogenizing annealing (Al-5083-0) before use in beam windows to remove the effects of prior working and defects, like slag inclusions or air holes, and to be less susceptible to radiation damage.

At the ISIS Target Station 2 (TS2) of the Rutherford Appleton Laboratory 5083 alloy is utilized for the proton beam window. Unlike the Target Station 1 PBW, where the design of a window with water flowing between two Inconel 718 plates had been adopted, a 0.5 mm-thick 5083-O aluminum alloy window with passive cooling by void vessel helium atmosphere was preferred for the more recent ISIS TS2. The Al-5083 window was in operation between 2008 and 2017, the year in which a failure occurred, leading to a 2-month shutdown of the beamline. A postirradiation examination of the window is scheduled with the purpose of obtaining a better understanding of radiation damage and embrittlement mechanism in PBW [77].

A 5083 alloy PBW is installed inside the spallation neutron source at J-PARC. The window, positioned 1.8 m upstream of the mercury spallation target, is used to separate the ultrahigh vacuum environment in the proton beam transport line from the target region filled with helium gas of 0.1 MPa [78]. As it can be seen in Fig. 12, in which the whole assembly of the PBW is shown, the window consists of 2.5 mm-thick aluminum alloy plates (sandwiched structure) with coolant water

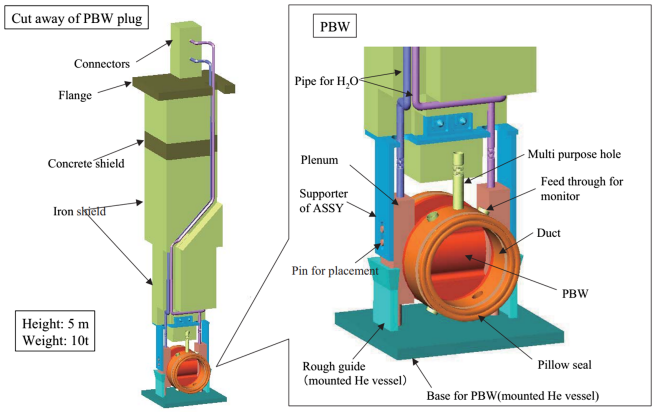

FIG. 12. Schematic drawing of the proton beam window of the spallation neutron source at J-PARC (JSNS) [78].

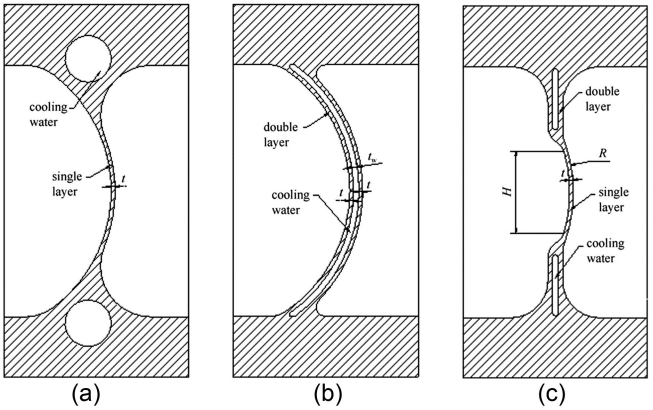

FIG. 13. The cross section of three PBW structures designed for CSNS: (a) single-layer structure. (b) Sandwiched structure. (c) Single-double layer structure [80].

flowing in a horizontal direction [79]. Initially, the intention was to utilize Inconel alloy as the window material, owing to its considerable structural strength. However, the optics calculation indicated that the beam scattering inside a window in Inconel 718 would have been too high and that a material with a lower atomic number was preferable. The aforementioned promising results obtained on the $AlMg_3$ alloy at PSI have directed the search in aluminum alloy materials and, finally, Al-5083 was chosen and used for the manufacturing of the PBW of the Japan Spallation Neutron Source (JSNS). It is noteworthy that, since the PBW is being highly activated during the beam operation and requires to be replaced every 2 years, a remote handling procedure was implemented for the replacement in order to minimize the shutdown period of the JSNS facility.

Finally, the 5083-O alloy was chosen as the PBW material of the China Spallation Neutron Source (CSNS). The CSNS is an accelerator-based neutron source built in Dongguan (Guangdong Province, China). The construction of the facility was completed in 2018 and the design aim of 100 kW (phase I) was achieved in 2020. A power upgrade is planned for the next years, from 100 kW of phase I to 500 kW of phase II, with an intermediate stage at 200 kW. The present CSNS PBW is used as a boundary to separate the high vacuum environment, where the 1.6 GeV proton beam comes from, and the helium-filled environment of the solid tungsten station, where neutron scattering experiments occur. The choice of Al-5083-0 for the proton beam window has followed a similar path to that of the JSNS PBW: both Inconel 718 and 5083 alloy have been compared and the latter has been considered more suitable for the purpose in light of a better scattering effect and a lower proton energy deposition (the heat deposition on Al-5083, calculated by SRIM software, has resulted to be one-third of that on Inconel 718) [80].

An extensively investigated aspect of the CSNS PBW design involves the analysis of the cooling structures. The design of the CSNS PBW introduces the advantages of the two more common PBW cooling structures: (i) The single-layer structure [Fig. 13(a)], the most suitable cooling structure for low beam power windows, has low-energy deposition, a small scattering effect, and a little water activation but a low capacity of thermal dissipation. (ii) The sandwiched structure [Fig. 13(b)] utilized for the spallation sources at the Oak Ridge National Laboratory and at J-PARC, which owns good strength, processability, and thermal dissipation ability for high beam power, but results in a serious activation of the cooling water as well as in a high-energy deposition and scattering effect.

The single-double layer structure [Fig. 13(c)], a compromise between the previous cooling structures, was proposed for the CSNS PBW in 2013 and installed in 2018. Now the window has been failure-free operated for several years and is planned to be replaced after 7 years of operation. Recent studies about the possibility of using this window design with a beam power of 200 kW show that the PBW must be changed despite the advantages of the single-double layer structure due to the excessive temperatures that would be reached [23].

The two mechanisms of radiation damage that most affect the mechanical properties and microstructure of the Al-Mg alloys are the formation of helium bubbles and the radiation-induced Mg-Si precipitation. The irradiation hardening (resulting in an increase in yield stress) and embrittlement (leading to a decrease in elongation) of these alloys are intricately dependent on the nature and intensity of the radiation.

The Al-5052 alloy, exposed to neutron irradiation at the High Flux Isotope Reactor, showed signs of hardening due to the formation of dislocation loops and small Mg_2Si precipitates [81]. Under the exposure of thermal neutron flux, aluminum can transmute into silicon through the following two-stage reaction:

$$^{27}\mathrm{Al}(n,\gamma) \rightarrow {}^{28}\mathrm{Al} \rightarrow {}^{28}\mathrm{Si} + \beta. \quad (8)$$

The Al-5052 alloy is thus continuously modified and converted to a ternary Al-Mg-Si alloy due to thermal neutron absorption and, because the solubility of silicon in aluminum is low, the transmutation-produced Si interacts with the Mg in the matrix to produce Mg_2Si precipitates.

On the other hand, under high-energy proton irradiation, as in the case of the $AlMg_3$ safety-hull irradiated at SINQ, the Mg_2Si precipitates could not be observed, but high-density small bubbles were detected [76]. The primary cause of high-density small bubble production may be ascribed to the high contents of helium and hydrogen produced by high-energy protons. Compared to the former case of neutron irradiation at HFIR, the helium production rate is nearly a thousand times greater and the formation of the bubbles was already observed at rather low irradiation doses (0.7 dpa) [81,82]. These small and dense bubbles are strong enough to obstacle the dislocation motion: their presence can enhance the effects of embrittlement and irradiation hardening on the window material. Since the irradiation embrittlement caused by a large amount of He bubbles is expected to have the most detrimental effect on the mechanical properties of aluminum alloys, the gas production is considered to be more appropriate than the dpa calculation for the lifetime estimation of an aluminum beam window [23].

2. Aluminum 6000-series alloys

The Al-Mg-Si alloys are precipitation-hardened alloys with the characteristic of being easy to machine, weldable, and equipped with good mechanical properties greatly dependent on the heat treatments. They find application in several fields and are used for the construction of aircraft structures and automotive parts as well as for different components in nuclear reactors, including reflector vessels.

Within the group of the 6000-series alloys, Al-6061 was selected to be adopted in beam windows applications. The 6000-series aluminum alloys have magnesium (0.8–1.2 wt %) and silicon as their major alloying elements (0.4–0.8 wt % Si). Small quantities of Fe, Cu, Cr, Ti, and Zn are added to improve aqueous corrosion resistance and mechanical strength and to control the grain size. The 6061 alloys may be heat treated to produce a finely distributed Mg_2Si phase precipitate to enhance both strength and ductility. Different temper states can be found on the market, including the annealed state (Al-6061-O) and the tempered grades T6 and T651. The designation "Al-6061-T6" denotes the application of a heat treatment that results in the dispersion of small needle-shaped precipitates, while the designation "Al-6061-T651" denotes the straightening treatment, which was applied to the alloy after quenching but before the heat treatment.

This precipitate-strengthened alloy was subjected to neutron and proton irradiation to assess the effects of radiation on the mechanical properties. Under neutron irradiation, 6061 alloys exhibited very high tensile strengths (about 350–400 MPa) and conserved sufficient ductility at high doses (70 dpa) [83,84]. No new grain bubbles were observed in the samples of Al-6061-T6 irradiated with 800 MeV protons at the Los Alamos Meson Physics Facility and the He bubbles detected along the Mg_2Si phase precipitates are likely to have been produced during the treatment of thermal aging [85].

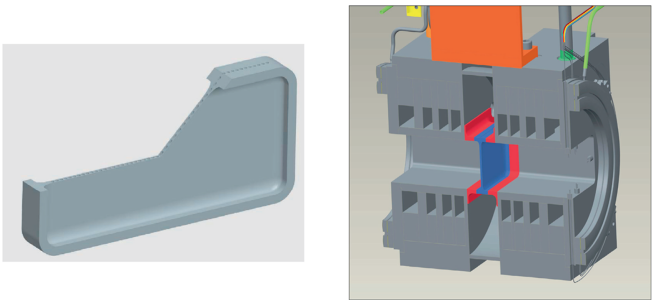

FIG. 14. Second generation Al-6061-T651 PBW at the spallation neutron source: (a) sectional view of flat-plate aluminum window and (b) cross-sectional view of complete SNS proton beam window assembly [18].

Due to the encouraging findings regarding the bubble formation and the preservation of ductility of this alloy after high-dose irradiation, thermally treated 6061 alloys were taken into account for beam windows applications.

Al-6061-T651 was selected for the second generation PBW at the Spallation Neutron Source at Oak Ridge National Laboratory to replace the first generation PBW made of Inconel 718. As can be seen in Fig. 14, the window consists of a 0.2-inch-thick flat aluminum plate with a series of small circular ducts (0.125 inches in diameter), which guarantee the dissipation of the thermal energy deposited by the proton beam through the passage of cooling water inside (the so-called multipipe cooling structure) [18].

The 6061-T6 alloy was eventually chosen as a structural material for the PBW of the European Spallation Source Target station, currently under construction in Lund, Sweden. The proton beam window will be installed inside the accelerator tube that will lead 2 GeV protons to a tungsten target, depositing a record value of around 5 MW of energy in a rotating He cooled wheel, as can be observed in Fig. 15(a). Initially, a multipipe design with a helium-based cooling system was proposed for the PBW [86]. This design concept was recently replaced with a water-cooled sandwiched structure, capable of providing larger cooling rates to evacuate all the power deposited (a considerable amount of energy of 6 kW, equal to around 0.1% of the total power, is expected) [87]. This new design of PBW, shown in Figs. 15(b) and 15(c), consists of two thin cylindrical plates (1.25 and 1 mm, respectively) separated by cooling channels. Since the passage of water can lead to undesired beam distortion (definitely higher than that of the helium-based cooling system proposed previously), a very thin

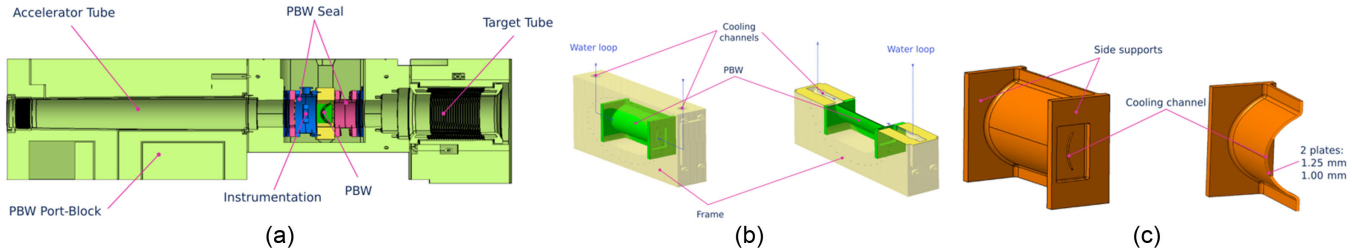

FIG. 15. Overview of the PBW assembly of the 5 MW ESS Target Station (a). Detail of the PBW welded to the frame (b) and without side supports (c) [87].

2 mm cooling channel, in which a 0.3 kg/s water flow rate circulates, is specially designed for this beam window.

The limited availability of radiation damage data under high-energy proton irradiation poses challenges in precisely determining the lifetime limit of new designs of PBWs in 6061 alloy. Examining the operational experience of similar windows in terms of gas production—the most appropriate indicator for radiation damage estimation of components in aluminum alloys—is the standard procedure for determining the lifetime limit. The administrative lifetime limit for the proton beam windows of the China Spallation Neutron Source and the SNS at the Oak Ridge National Laboratory was established on the basis of the results of the postirradiation measurements carried about at PSI on the SINQ safety-hull assemblies, fabricated from $AlMg_3$. Since no evidence of component compromise was found at the end of their operational lifetime, the observed level of He production (2000 appm He) was set as a conservative limit for the SNS windows in 6061 alloy [18,23]. Likewise, the data of the postirradiation examinations on the SINQ target-9 safety hull at PSI were used as a guideline for assessing the lifetime of the PBW at ESS [88]. The entrance window of target 9 was exposed to the irradiation of high-energy proton beams and backscattered neutrons to the extent that, according to the neutronic simulations performed, the maximum values of displacement damage (8.5 dpa) and helium production (2450 appm) ever recorded in spallation target environments were reached [89]. Recent tensile tests on samples extracted from the entrance window revealed that $AlMg_3$ exhibits brittle behavior with a reduced total elongation (2%) at this level of radiation damage (8.5 dpa) [90]. In order to avoid sudden brittle fracture, a more conservative helium concentration level (2400 appm) was proposed as the lifetime administrative limit for the ESS proton beam window [88].

Table XII presents examples of Al-alloy windows installed in spallation sources with respective beam parameters and cooling structures.

IV. OTHER NONMETALLIC MATERIALS

The need to respond to the challenges presented by future high-power and high-intensity accelerator facilities

TABLE XII. Beam parameters and cooling structure of PBWs of spallation sources in Al-alloy.

	Research center	Beam power	Proton energy	Proton per pulse	Rep. rate	Cooling structure
$AlMg_3$						
Safety-hull of the SINQ Target-3	Paul Scherrer Institut		0.57 GeV	Continuous beam		Double wall cooling by heavy water
A5083						
ISIS Target Station 2	Rutherford Appleton Laboratory	0.2 MW	0.8 GeV	2.8×10^{13}	50 Hz	Passive cooling, He
JSNS PBW	J-PARC	1 MW	3 GeV	8.3×10^{13}	25 Hz	Surface cooling
CSNS PBW (phase I)	China Spallation Neutron Source	0.1 kW	1.6 GeV	1.6×10^{13}	25 Hz	Single-double layer
A6061						
SNS PBW (2 gen)	Oak Ridge National Laboratory	1.4 MW	1 GeV	1.5×10^{14}	60 Hz	Multipipe cooling
PBW at ESS Target Station	European Spallation Source	5 MW	2.0 GeV	1.0×10^{15}	14 Hz	Water-cooled sandwich structure

TABLE XIII. Relevant nuclear, physical, and mechanical properties of carbon-based materials used in beam-window applications. The data on glassy carbon refer to the grade G, produced by Hochtemperatur-Werkstoffe (HTW) [92]. SB 1001G and SB 1501G refer to two grades of SIGRABOND Carbon Fiber-Reinforced Carbon, produced by SGL Carbon [93].

	GlassyC	SB 1001G	SB 1501G
Atomic number	6	6	6
Mass number	12.1	12.1	12.1
Radiation length ($g\,cm^{-2}$)	43.33	43.33	43.33
Density ($g\,cm^{-3}$)	1.42	1.36	1.47
Thermal conductivity ($W\,m^{-1}\,K^{-1}$)	6.30	116.67	19.60
Specific heat capacity ($J\,g^{-1}\,K^{-1}$)	0.85	0.71	0.71
Volumetric CTE ($10^{-6}\,K^{-1}$)	2.60	3.03	3.65
Melting temperature (°C)	3652	3652	3652
Young's modulus (GPa)	32.4	45.75	56.25
Poisson's ratio	0.155	0.15	0.15
Tensile strength (MPa)	112	93.3	331.7

has encouraged the scientific community to promote research programs even on novel nonmetallic materials.

The metals, which represent nearly the totality of the beam-window materials adopted in the wide variety of particle accelerator applications, possess typically many desirable features, such as high thermal conductivity and high mechanical strength; nevertheless, for some specific applications in which the distortion of the beam transversing the window and its opacity are the major issues, as is the case of the transmission of low-energy electrons and photons, very light materials with an atomic number lower than that of the metals (except for beryllium) are essential to keep up with the technological evolution pace.

This section aims to outline the nonmetallic materials currently in use for beam-window applications and to introduce the novel materials involved nowadays in research campaigns, anticipating possible future purposes.

A. Carbon-based materials

Carbon-based materials are the most promising nonmetallic materials for future beam-window applications, owing to their lightness (second only to beryllium) and outstanding physical properties in some of the various allotropic forms. Since there are numerous ways in which the carbon atoms can bond, many forms of allotropes can form, including graphite, diamond, and fullerenes, with properties radically different or opposite to one another. For example, graphite is a good electrical conductor but is fairly brittle due to the very weakly bounded layers of which it is composed, while diamond is a poor electrical conductor but is the hardest naturally occurring material known. The most attractive carbon materials for window applications are described below [91]. Relevant properties of carbon-based materials used in beam windows are listed in Table XIII.

1. Graphite and carbon-carbon composites

Graphite is a naturally occurring crystalline form of the element carbon that represents the most stable form of carbon under standard conditions. The properties of this allotropic form of carbon depend deeply on its crystallographic structure: each carbon atom contains three covalent bonds (σ bonds) directed to three other carbon atoms in the same plane as a result of the sp2 hybridization of the carbon atoms, while the fourth valence electron—not involved in the sp2 hybridization—is delocalized through π-π interaction. The result is a structure consisting of stacked hexagonally arranged sheets of carbon (graphene), with strong covalent bonding within the layer and adjacent layers weakly bonded through van der Waals forces [91]. Due to its extreme anisotropy, graphite exhibits noticeable differences in mechanical, electrical, and thermal properties among in-plane and out-of-plane directions. Therefore, graphite has desirable properties for beam windows in the in-plane direction, such as extraordinarily high elastic modulus and thermal conductivity and low coefficient of thermal expansion, but these characteristics are overturned in the other direction, due to the weakness of the van der Waals forces in bonding the different layers. Furthermore, the use of graphite is well established in the nuclear field and its properties have been closely examined under irradiation in numerous experiments over the last few decades. Typical applications are those of neutron moderators in nuclear power plants and of beam intercepting devices in the accelerator complexes, such as beam dumps or absorbers [94–97].

In order to exploit the excellent thermal and mechanical characteristics of graphite and overcome the brittleness issues due to its crystal structure, carbon-carbon composites have been used for beam-window applications, especially for the exit beam windows of the most modern accelerator facilities at CERN. These carbon-carbon composites are a class of materials composed of carbon fibers embedded into a carbon (or graphite) matrix. The reinforcement provided by the continuous carbon fibers not only significantly diminishes the brittleness of graphite but also leverages its attractive properties alongside the excellent versatility, strength, toughness, and thermal resistance of composites. The fabrication of these advanced thermostructural materials requires specific and elaborate methods—including thermal treatments and repeated carbonization and impregnation processes—which make these materials very costly and affordable only for elevated temperature applications in aerospace (rocket nozzles, space shuttle nose tips, etc.) and military fields [98].

These materials possess, however, two main drawbacks that limit their use: porosity and low oxidation resistance. The first issue arises from the presence of voids in the

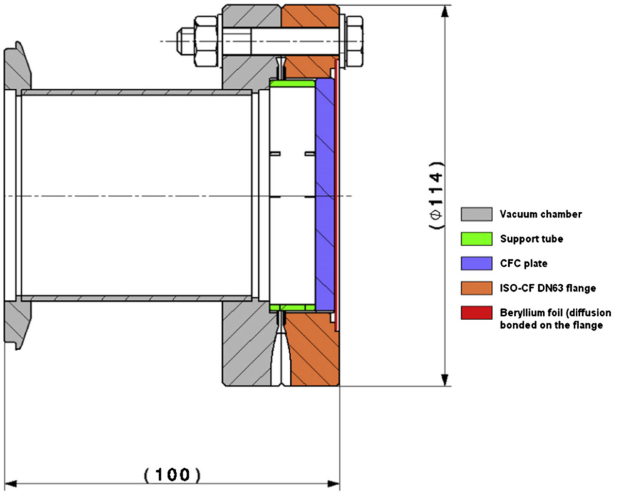

FIG. 16. CAD drawing of the vacuum double-layer beam window of the HiRadMat facility [2].

composite material's matrix: the most advanced and high-cost manufacturing techniques effectively reduce the number of defects, but nevertheless, there is no ultra-high vacuum leak-tight form of C-C currently existing in the industrial market. The poor oxidation resistance is instead due to the high reactivity that carbon has with oxygen in the air, especially at temperatures above 500 °C. The oxidation products, typically carbon monoxide and carbon dioxide, can be formed on the external surfaces of the composite as well as inside the material because of the numerous internal pores introduced during the manufacturing procedures.

As mentioned above, carbon-carbon materials have been employed for vacuum beam windows of the CERN accelerator facilities over the last 20 years [2,10,27,60]. To overcome the drawbacks mentioned above and to meet the vacuum requirements without ceasing to exploit the advantages offered by carbon-carbon composites, a double-layer design has been developed. This design solution consists of applying a thin impermeable leak-tight metallic foil (with a thickness of around 100th of an inch) on a thicker C-C layer. An example of this double-layer design is shown in Fig. 16, which represents the assembly of the HiRadMat facility, including window, flange, and vacuum chamber [2]. As can be observed, the impermeable metallic foil is installed on the high-pressure side: this arrangement forces the foil to adhere to the surface of the supporting C-C plate due to the pressure differential and prevents air penetration into the porosity of the composite material and, with this, its potential oxidation.

A few examples of CERN beam windows with this distinctive double-layer design are summarized in Table XIV. Two grades of carbon-carbon composites were used for CERN beam windows: Sigrabond 1001G and Sigrabond 1501G. These advanced materials, supplied by the company SGL Carbon, have low density (1.5–1.7 $g\,cm^{-3}$) and large radiation length ($X_0 \approx 29$–31 cm), low—especially planar—coefficients of thermal expansion, but relatively high coefficients of permeability (7×10^{-2} and 5×10^{-2} $cm^2\,s^{-1}$ for 1001G and 1501G type, respectively) for vacuum applications [93].

2. Glassy carbon

Another carbon-based material recently investigated to be adopted in beam windows is glassy carbon. It is a form of carbon with a highly disordered structure, obtained from a highly reticulated resin. This advanced material combines glassy and ceramic properties with graphitic ones. On one side, glassy carbon shares many outstanding properties with graphitic materials, such as high radiation length, low elastic modulus, low coefficient of thermal conduction and, most importantly, extreme resistance to thermal shock. On the other side, it is an isotropic material, impermeable to gasses and liquids and extremely resistant to corrosion. Its zero porosity and good oxidation resistance make this isotropic material very promising for vacuum applications.

Glassy carbon has been subject to numerous experimental campaigns at the High-Radiation to Materials Facility at

TABLE XIV. Features of double-layer vacuum beam windows designs at CERN [2,10,27,60].

		Accelerator facilities at CERN			
		LHC	CLIC	HiRadMat	CNGS
Proposed designs for double-layer beam windows		Beam dump beamline	Beam dump beamline	LHC to HiRadMat connection beamline	Proton beam exit window
Shape		Circular	Raceback square	Circular	Circular
Upstream layer	Material	Sigrabond 1501G	Sigrabond 1501G	Sigrabond 1501G	Sigrabond 1001G
	Thickness (mm)	15	15	5	2.5
	Diameter (mm)	600	260 × 500	70	68.5
Downstream layer	Material	AISI 316L	Aluminum	Be PF-60	Beryllium
	Thickness (mm)	0.2	0.2	0.254	0.254
	Diameter (mm)	600	260 × 500	70	60

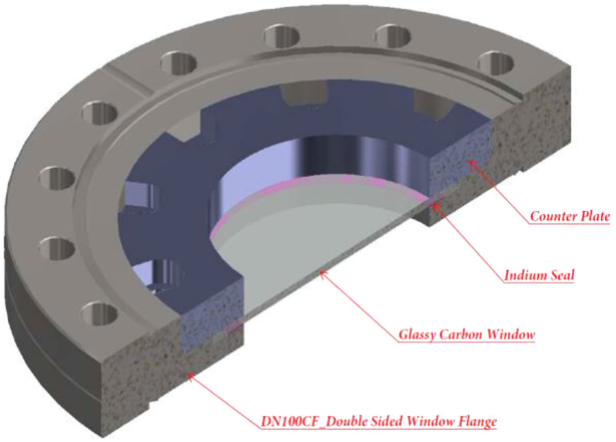

FIG. 17. CAD drawing of one glassy carbon beam window tested at the HiRadMat facility [100].

CERN since 2015. The irradiation tests are intended to investigate the thermomechanical and dynamic behavior of glassy carbon beam windows in case of impact of high-energy proton beams. Postirradiation examinations have been used to reveal the possible damages on the materials exposed to proton irradiation, while numerical simulations enable estimating to what extent the physical and mechanical properties have been changed. The materials for the experiments were supplied by Hochtemperatur-Werkstoffe (HTW) in two different grades, G and K, which exhibit different properties according to the heat treatment received. Grade G was selected for the irradiation campaign and its characterization was carried out before being exposed to the proton beam [92,99]. For the HRMT-26 experiment held in 2016, seven windows in glassy carbon were mounted inside the experimental beam-line to six volumes, either at atmospheric pressure or under vacuum. The CAD drawing of one tested window is shown in Fig. 17. The results of the irradiation with 440 GeV proton pulsed beams demonstrate that all the windows can withstand the heat deposition from both thermal and mechanical standpoints. However, the postirradiation studies reveal mechanical damage: several cracks on the fourth window on both faces compromise the window's vacuum tightness. The onset of a volumetric swelling, observed in the irradiated area and probably attributable to helium and hydrogen generation in the inner substance, could make some changes to the mechanical properties of the material and undoubtedly demand further investigations [100,101]. In the subsequent HRMT35 experiment, an irradiated window reported failure signs, probably due to the badly designed flange that prevented the radial expansion of the beam window, but vacuum performance was not compromised [102]. Finally, detailed investigations on glassy carbon samples are scheduled at CERN (SMAUG experiment) for the purpose of gaining a better understanding of the thermomechanical behavior of this and other materials under the impact of even higher energy pulsed proton beams [37].

B. Ultrathin beam windows

The concept of ultrathin windows for high-power hadron beam accelerators appeared relatively recently in response to the demand for excellent particle transmissivity and minimal heat deposition. Electron microscopy, x-ray fluorescence analyzers and x-ray instrumentation for space missions are just some of the fields where membrane beam windows are employed. The advanced materials selected for this purpose must possess the typical characteristics for beam-window applications (high mechanical strength, low-Z, extremely high thermal conductivity, radiation tolerance, etc.). At the same time, the conditions of leak-tightness and vacuum performance must be met despite the very limited thickness of the membrane (usually around 1 μm) [103]. The most promising materials for this type of application are graphenic carbon, silicon nitride, and silicon carbide. In the field of soft x-ray applications, polymeric windows are widely used, because of the intrinsic elastic nature that enables them to tolerate pressure difference and the excellent x-ray transmission. However, their implementation for high-energy hadron beams is impracticable because of their low resistance at high temperatures and imperfect leak tightness for UHV conditions [104].

Silicon nitride (Si_3N_4) and silicon carbide (SiC) have been recently considered interesting for the design of the window for ionising cooling for the hypothetical Muon Collider at CERN. The low energies involved require the thinnest possible windows (< 100 mm) to minimize the rather strong interaction of muons with the window material. Silicon carbide, a material widely utilized material in the semiconductor industry and in x-ray transmission applications, possesses numerous excellent properties, such as remarkable strength as compared with its thickness, uniformity, gas tightness, and capability to be manufactured in ultrathin thicknesses (up to 10 nm). It can work at cryogenic temperatures and can withstand differential pressure above 1 bar without failure [105]. On the other hand, membranes in SiC exhibit thermal conductivity four times that of silicon nitride and superior transmission characteristics, but its technology is currently less mature [106]. A Si_3N_4 window is planned to be investigated under proton irradiation in the HRM-59 Windows Experiment at CERN [37].

Finally, graphenic carbon stands out as the most promising ultrathin material for high-power hadron windows, presenting itself as an excellent alternative to conventionally adopted window materials in accelerator-driven systems and spallation neutron systems. Graphene is an allotrope of carbon that consists of a single carbon layer and has excellent mechanical properties, high strength up to 130 GPa and extremely high thermal conductivity, up to 5300 W/mK. Furthermore, the high chemical stability of these membranes, their high gas tightness, and their impermeability make them suitable for vacuum applications. Nowadays, their use as vacuum window material is well established in several fields, such

as electron microscopy and x-ray photoelectron spectroscopy [107]. However, more detailed investigations must be performed before graphenic carbon membranes may be used in real vacuum window applications, especially on the resistance to radiation and vacuum performance. Recent studies on the subject have been carried out at the Institute of High Energy Physics in Beijing and at the AVF accelerator at RIKEN, the Japanese Institute of Physical and Chemical Research. Regarding the research held at IHEP, thermomechanical and particle transport simulations were carried out in the first place in the hypothesis of replacement of the A5083-O proton beam window at China Spallation Neutron Source. A proton beam of 1.6 GeV at different beam powers (ranging from 1 up to 50 MW) was assumed to impact onto a square window with a thickness equal to 335 nm (100 layers of graphene). The numerical results show very low maximum temperatures (due to the excellent thermal diffusivity of graphene and the ultrathin thickness), which translate into minimal beam-induced mechanical stresses [108]. Follow-up studies have focused on the vacuum performance of graphene films, through tests in which graphenic carbon windows have been subjected to a differential pressure of 1 bar between a vacuum environment and a helium-filled one: 100 μm-thick graphene film has shown a great impermeability to helium and the recorded leak rate is at the same level of the proton beam window requirement of CSNS, thus proving the excellent gas leak-tightness of this promising material [109]. The primary objective of the research held at RIKEN is to investigate the extraordinary mechanical properties of this ultrathin material and to study how they evolve when exposed to the conditions of a highly radioactive environment. Five graphenic carbon samples of thickness 1 μm and diameter 7.5 mm were irradiated at different levels of fluence and for different time intervals using 5 MeV/u ^{20}Ne ion beam from the AVF accelerator at RIKEN. The foils, capable of mechanically withstanding the 200 particle nA dc beam for 10 h, are being investigated in detail at the University of Münster and at the GSI Helmholtz Center for Heavy Ion Research to identify the radiation-induced damages and to assess the eventual change of the mechanical properties. The successive step is to evaluate the vacuum performance of these samples (under a differential helium pressure of 0.2 MPa) during irradiation by monitoring the helium leakage through the window [110]. The outcomes of these and further experiments are essential to demonstrate the feasibility of graphenic carbon windows for upcoming applications with high-energy and high-luminosity hadron beams.

V. MATERIALS CLASSIFICATION: FIGURES OF MERITS AND OTHER INDICATORS

A. The thermomechanical robustness index

The thermomechanical robustness index (TRI) is associated with the mechanical robustness of the material and serves to give qualitative information on the material's ability to withstand the impact of a short particle pulse.

Considering that thermal shock problems are largely dictated by the thermal deformation caused by a fast temperature increase, it seems appropriate to build this index on the ratio between material admissible strain (or strain to failure) $\varepsilon_{\mathrm{adm}}$ and actual reference strain $\varepsilon_{\mathrm{ref}}$:

$$\mathrm{TRI} = \frac{\varepsilon_{\mathrm{adm}}}{\varepsilon_{\mathrm{ref}}}\left(\frac{T_{\mathrm{melt}}}{\Delta T_{\mathrm{q}}} - 1\right)^{m}, \tag{9}$$

where T_{melt} (K) is the melting (or degradation) temperature, ΔT_{q} (K) is the temperature increase generated by a reference energy deposition [Eq. (12)], and m a coefficient related to the material loss of strength when the temperature increases.

The actual reference strain is defined by

$$\varepsilon_{\mathrm{ref}} = \bar{\alpha}\Delta T_{\mathrm{q}}, \tag{10}$$

where $\bar{\alpha}$ (10^{-6} K) is the (averaged) coefficient of thermal expansion and ΔT_{q} the temperature increase generated by a reference quasi-instantaneous energy deposition q_{d}, which can be expressed as a function of the material density ρ (g cm^{-3}), the specific heat c_{p} (J g^{-1} K^{-1}), the scaling factor C_{R}, the coefficient n, which indicates how density affects the energy distribution generated by the impact, and the geometrical radiation length X_{g} (cm):

$$q_{\mathrm{d}} = \frac{C_{\mathrm{R}}\rho^{\mathrm{n}}}{X_{\mathrm{g}}}, \tag{11}$$

$$\Delta T_{\mathrm{q}} = \frac{q_{\mathrm{d}}}{c_{\mathrm{p}}} = \frac{C_{\mathrm{R}}\rho^{\mathrm{n}}}{c_{\mathrm{p}}X_{\mathrm{g}}}. \tag{12}$$

The radiation length in the previous formula provides an important indication of the "transparency" of a certain material to radiation: it is defined as the mean length (cm) required to reduce the energy of an electron by a factor $1/e$ [6]. The radiation length X_0, expressed in g cm^{-2}, can be approximated by the analytical formula below:

$$X_0 = \frac{716.4A}{Z(Z+1)\ln(\frac{287}{\sqrt{Z}})}. \tag{13}$$

The radiation length in cm is obtained by dividing by the density:

$$X_{\mathrm{g}} = \frac{X_0}{\rho}. \tag{14}$$

The value of the strain to failure ($\varepsilon_{\mathrm{adm}}$), i.e., the measure of how much the material is elongated to failure, is rarely available for many materials, so it is convenient to express this quantity as a function of values generally easier to find

in the literature, such as the (averaged) Young's modulus $\bar{E}$ (GPa), the Poisson's ratio ν, and the failure strength R_M (MPa). For simplicity, the ultimate tensile strength was utilized to describe the failure strength, despite the latter value being usually related to fracture for brittle materials and to yield strength for ductile ones. The admissible strain is therefore computed by the following relation:

$$\varepsilon_{adm} = \frac{R_M}{\bar{E}(1-\nu)}. \tag{15}$$

Combining the previous equations, the Thermomechanical Robustness Index can be finally written as

$$TRI = \frac{R_M\, c_p\, X_g}{\bar{E}(1-\nu)\,\bar{\alpha}\, C_R\, \rho^n}\left(\frac{T_{melt}\, c_p\, X_g}{C_R\, \rho^n} - 1\right)^m. \tag{16}$$

It is worth noting that, as the melting point is reached, TRI tends to zero.

B. The thermal stability index

The thermal stability index (TSI) indicates a material's capacity to preserve geometrical stability and minimizing deformation when subjected to steady-state beam losses.

When heat is deposited locally inside a small portion of matter in a larger body, as is the case of the components which intercept high-energy charged particle beams, a deflection of the structure is thermally induced, as shown in Fig. 18 for an LHC secondary collimator jaw. Assuming that this heat deposition is steady state and that the heat is flowing from the surface exposed to the beam through the thickness of the component, then the index TSI is developed to be proportional to the radius of curvature ρ_c of an elongated structure induced by a nonuniform temperature distribution:

$$\rho_c = \frac{\bar{\lambda}}{\dot{q}\,\bar{\alpha}}, \tag{17}$$

where $\bar{\lambda}$ ($W\,m^{-1}\,K^{-1}$) is the (averaged) thermal conductivity and $\dot{q}$ ($W\,m^{-2}$) the steady-state heat flux deposited on the structure:

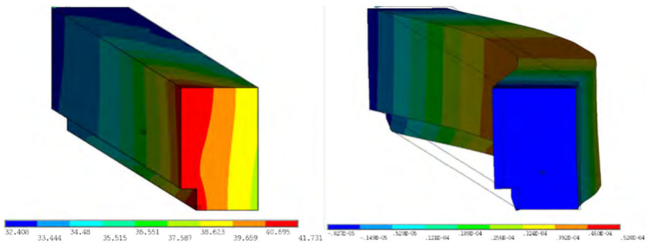

FIG. 18. Operating temperatures (°C) (left) and thermally induced deflection (m) (right) of an LHC secondary collimator jaw in steady-state conditions [111].

$$\dot{q} = \frac{C_S\, \rho^n}{X_g}, \tag{18}$$

where C_S represents a scaling factor.

Combining Eqs. (17) and (18), the thermal stability index can be finally written as

$$TSI = \frac{\bar{\lambda}\, X_g}{\bar{\alpha}\, C_S\, \rho^n}. \tag{19}$$

C. Evaluation of analyzed materials

A comparison of the materials for beam-window applications presented in the previous sections is provided by the bar chart in Fig. 19. The values of the figures of merit (FoM) shown in the graph were evaluated by reference to the physical and mechanical properties presented in Tables I–XIII. The latter tables are evidently representative of material properties at standard conditions at room temperature ($T_{room} = 20°$), except for the coefficient of thermal expansion (CTE), which was averaged between 20° and 100° in most cases. Moreover, for transversely anisotropic materials, such as the carbon fiber-reinforced carbon composites, the values presented in these tables and used for the evaluation of the figures of merit were estimated through the following formula: value $= [2 \times (\text{best direction}) + (\text{weak direction})]/3$. In this regard, it is good to remember that FoMs must be treated as qualitative parameters to be used for a relative comparison between the selected materials.

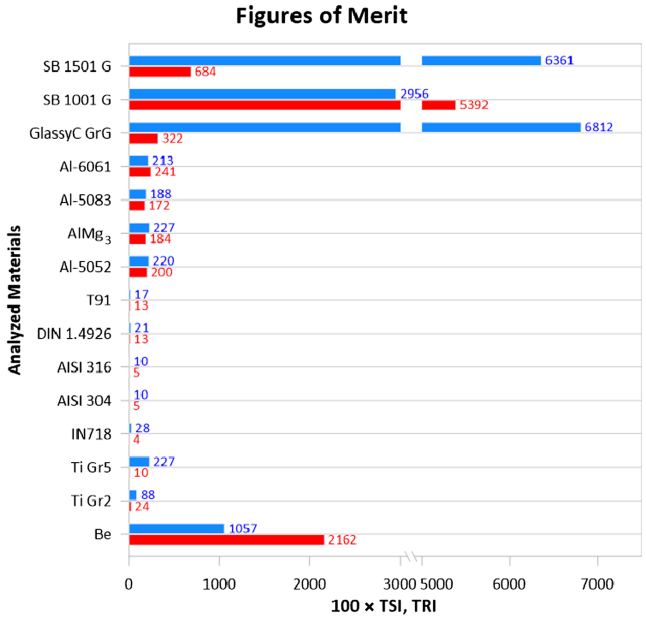

FIG. 19. Comparison of the thermomechanical robustness indices (TRI, in blue in this figure) and thermal stability indices (TSI, in red in this figure) estimated for various beam window materials.

From the first glance of the graph, it is immediately noticeable that beryllium and carbon-based materials possess the highest values of TRI and TSI. The low-Z, the low density, and the outstanding thermal conductivity are the reasons why beryllium has the highest TSI and TRI among the metallic materials, despite the not exceptional value of the coefficient of thermal expansion, quite in line with those of the stainless steels. These findings reveal the excellent qualities of this material for BIDs and explain the keen scientific interest that collects in many international research projects notwithstanding the critical issues of oxidation, manufacturability, and toxicity relating to its use. Values of TRI and TSI comparable to beryllium ones are owned just by carbon-based materials, by their low density, reduced thermal expansion coefficient, and extraordinarily high degradation temperature. Using the example of glassy carbon, a direct comparison with beryllium shows a larger thermomechanical robustness index in the carbon-based material, due to its higher degradation temperature and its lower elastic modulus and CTE, but a lower thermal stability index, especially because of the thermal conductivity coefficient, more than 30 times smaller than the Be's one.

Among the other materials, aluminum alloys offer the best characteristics in terms of TRI and TSI. Their key advantages lie in the exceptional thermal conductivity and the relatively high specific heat capacity, while the main drawbacks are the low coefficient of thermal expansion and the extremely low melting temperature (around 600 °C), which makes the design of cooling structures indispensable to prevent creep failures and which constitutes a barely acceptable engineering constraint for the next generation of high-intensity acceleration facilities.

The values of the FoM evaluated for titanium alloys are not very high, and the main reason lies in their extremely reduced thermal diffusivity, an important metric for beam-window applications since it embodies the capacity of propagating the heat deposited inside the material by the particle beam toward the edge, thus avoiding that it accumulates at the center and that unbearable temperatures are reached. However, Ti-6Al-4V possesses a TRI of around 200, comparable with that of aluminum alloys by its excellent tensile strength.

The Ni-based superalloy Inconel 718 shares the same faults as titanium alloys in terms of thermal diffusivity, but does not have the same lightness. In this case, the ΔT_q, i.e., the temperature increase generated by a reference quasi-instantaneous energy deposition, turns out to be the highest one among all the materials considered, with a value of around 45.96 °C, far higher than the 0.46 °C of beryllium. All this is reflected in the values of the two figures of merit, especially in the TSI. The main quality of this metal is the outstanding value of the failure strength ($R_M = 1375$ MPa), the highest among all the materials, thanks to which its TRI is greater than the ones of the stainless steels. Finally, the stainless steels exhibit the lowest values of TSI and TRI among the materials selected. Short radiation length, high Young's modulus, and reduced specific heat capacity are the main causes of this result. Additionally, due to their higher thermal diffusivities and lower coefficients of thermal expansion, martensitic steels are revealed to be more appropriate as beam-window materials than austenitic ones, with values of TRI and TSI 2 and 3 times higher, respectively.

VI. CONCLUSIONS

The identification and selection of structural materials suitable for beam-window applications is an essential factor in enhancing the performance of next-generation accelerator facilities as well as in ensuring their safe and optimal operation. Within the wide field of components for accelerator systems, the beam windows are undoubtedly one of the most critical components as well as one of the elements that experience failures more frequently throughout a facility's lifetime. The large variety of beam intensities, the application of thermomechanical and pressure loads of different entities, and many other specific conditions led to a wide range of constructive solutions, which share many commonalities and which is of fundamental importance to know before proceeding with the project of new beam windows. The ambitious purpose of the article is precisely to provide a first instrument for guiding the design choice of beam-window materials in light of the increasingly stringent requirements associated with this component in future higher-intensity and higher-energy accelerator facilities.

The literature research took into account the strengths and weaknesses of each beam-window material, focusing on their behavior in terms of thermal shock response and radiation damage when exposed to particle beams. The beam-window applications of each material in accelerator facilities and research centers of internationally recognized importance were described, and plans for future installations or experiments were also reported. Additionally, this search process contributed to providing an organic and rational overview of all the materials for beam-window applications, which was followed by the introduction of two figures of merit—thermomechanical robustness index and thermal stability index—capable of providing a useful comparative indicator of the performance of each material under beam irradiation.

This material comparison suggests that beryllium and carbon-based materials exhibit excellent thermomechanical characteristics, significantly better than the ones of the other materials, in terms of the ability to withstand the impact of short-pulsed beams (high values of TRI) and steady-state beams (high values of TSI). Quite high values of the two FoMs are then exhibited by the aluminum alloys, by virtue of their low density and exceptional thermal conductivity, followed by titanium alloys, Inconel 718, and,

finally, stainless steels. Nevertheless, even the materials that excel in this comparison are not entirely devoid of critical issues, issues that were overlooked by the previous indices—such as those related to their radiation-induced damage, machinability, and corrosiveness—and that are no less important in the design choice. For instance, the strong toxicity of beryllium has prompted recent considerations regarding the replacement of this structural material inside the beamlines, and this involves in particular the beam windows, critical components that often experience sudden failures throughout the facility's lifetime.

The design of each beam window is closely connected with the specific needs required by the environment in which it is installed. The entrance or exit beam windows of the accelerator facilities' beamlines are composed of beryllium, titanium alloys, carbon-carbon composites, or austenitic steels. These are generally materials that have very high melting temperatures that do not require active cooling systems and that have low nuclear interaction cross sections. Single-layer windows in AISI 304, Al-5052, and titanium grade 2 are nowadays considered inadequate for the higher-intensity particle beams of the upcoming accelerator facilities, while Ti-6Al-4V is extensively used at FNAL and J-PARC, even for future applications. At CERN, the most common design for new windows consists of multilayer structures, where an impermeable metallic foil—usually made of stainless steel AISI 316L or Ti-6Al-4V—is forced to adhere on the surface of a supporting C-C plate. This arrangement makes it possible to exploit the outstanding properties of the carbon materials and, at the same time, preserve the leak tightness of the component.

On the other hand, the proton beam windows of the accelerator-based neutron source facilities, such as the spallation neutron sources and the future subcritical reactors, prefer the use of materials capable of withstanding the severe irradiation conditions typical of the atmosphere around the target assembly. The most commonly used materials are Inconel 718, because of its high corrosion resistance, excellent tensile strength, and adaptability to extreme environments, and aluminum alloys, by their low-energy deposition, low effect on beam scattering, and good thermal conductivity. 5083-O alloy is the most widespread (CSNS, JSNS, and ISIS), while Al-6061-T6 was selected as a structural material for the PBW of the European Spallation Source, currently under construction. The martensitic stainless steel T91 appears to be suitable for beam-window applications in future accelerator-driven subcritical reactors on account of its strong corrosion resistance and its good creep rupture strength.

Finally, in response to the demand for excellent particle transmissivity and minimal heat deposition, a novel idea of a beam window made with membrane materials has emerged in recent times. These materials (silicon nitride, silicon carbide, graphene, etc.) possess physical and thermomechanical properties equal, if not superior, to the ones of the conventional materials for beam windows. However, their behavior under particle radiation, thermal shock conditions, or pressure difference is still unpredictable, which is why their use as a vacuum window material is currently being explored in various experimental campaigns, even given future replacements of conventionally adopted windows at the end of their lifetime.

ACKNOWLEDGMENTS

The work behind this publication has received funding from the European Union's Horizon 2020 Research and Innovation Program under Grant Agreement No. 101004730.

[1] H. Wang, C. Meng, H. Qu, X. Sun, P. Wang, and D. Zhu, in *Proceedings of the 9th International Particle Accelerator Conference, Vancouver, BC, Canada* (JACoW, Geneva, Switzerland, 2018), p. 4.
[2] M. Monteil, J. Blanco, and R. Veness, Vacuum **85**, 1165 (2011).
[3] C. Meng, J. Y. Tang, and H. T. Jing, High Power Laser Part. Beams **23**, 2773 (2011).
[4] C. Johnstone, C. Gattuso, M. J. Syphers, and K. Paul, in *Proceedings of the 20th Particle Accelerator Conference, PAC-2003, Portland, OR* (IEEE, New York, 2003).
[5] A. A. Correa, Comput. Mater. Sci. **150**, 291 (2018).
[6] M. Gupta, Calculation of radiation length in materials, CERN Technical Report No. PH-EP-Tech-Note 2010-013, 2010.
[7] H. Hotchi, AAPPS Bull. **31**, 23 (2021).
[8] H. Klein, in *Proceedings of the 17th International Linear Accelerator Conference (LINAC-1994), Tsukuba, Japan* (KEK, Tsukuba, Japan, 1994), p. 6.
[9] G. S. Bauer, Nucl. Instrum. Methods Phys. Res., Sect. A **463**, 505 (2001).
[10] A. Ferrari and V. Ziemann, Conceptual design of a vacuum window at the exit of the CLIC post-collision line, CERN Technical Report No. EUROTeV-Report-2008-009, 2008.
[11] C. Murdoch, A. Decarlo, S. Henderson, S. Kim, K. Potter, T. Roseberry, J. Rank, and D. Raparia, in *Proceedings of the 2003 Bipolar/BiCMOS Circuits and Technology Meeting, Portland, OR (IEEE Cat. No.03CH37440)* (IEEE, New York, 2003), Vol. 3, pp. 1467–1469.
[12] H. Wang, H. Jing, H. Qu, and J. Tang, in *Proceedings of the 5th International Particle Accelerator Conference, IPAC-2014, Dresden, Germany*, (JACoW, Geneva, Switzerland, 2014), p. 3.
[13] C. Ader, M. Mcgee, L. Nobrega, and E. Voirin, in *Proceedings of the 9th International Particle Accelerator Conference, IPAC-2018, Vancouver, BC, Canada* (JACoW, Geneva, Switzerland, 2018).
[14] J. L. Western, Mechanical safety subcommittee guideline for design of thin windows for vacuum vessels, FERMILAB Technical Report No. FERMILAB-TM-1380, 1993.

[15] R. Roark and W. Young, *Roark's Formulas for Stress and Strain* General Engineering Series (McGraw-Hill, New York, 1989), 6th ed., p. 763.

[16] M. Monteil, Vacuum windows, CERN Technical Report, 2010, https://indico.cern.ch/event/114535/?print=1&view=event.

[17] C. Accettura, Investigation of radiation damage effects in HL-LHC collimator materials, Ph.D. thesis, Politecnico di Milano, 2021.

[18] D. A. McClintock, J. G. Janney, and C. M. Parish, J. Nucl. Mater. **450**, 163 (2014).

[19] G. S. Was, in *Fundamentals of Radiation Materials Science: Metals and Alloys. Irradiation Hardening and Deformation*, edited by G. S. Was (Springer, Berlin, Heidelberg, 2007), pp. 581–642.

[20] X. Xiao, Metals **9**, 1132 (2019).

[21] C. R. Ader, M. Alvarez, J. S. Batko, R. Campos, M. W. McGee, and A. Watts, in *Proceedings of the 10th International Particle Accelerator Conference, IPAC-2019* (JACoW, Geneva, Switzerland, 2019), p. 3, https://doi.org/10.18429/JACoW-IPAC2019-WEXXPLS2.

[22] A. Žohar, I. Lengar, and L. Snoj, Fusion Eng. Des. **160**, 111828 (2020).

[23] H. Wang, D. Zhu, L. Kang, P. Wang, H. Jing, Y. Liu, L. Zong, and H. Qu, Nucl. Instrum. Methods Phys. Res., Sect. A **1042**, 167448 (2022).

[24] C. Ader, in *Proceedings of the 9th International Particle Accelerator Conference, IPA-C2018, Vancouver, BC, Canada* (JACoW, Geneva, Switzerland, 2018), p. 25.

[25] Y. Dai, C. Fazio, D. Gorse, F. Gröschel, J. Henry, A. Terlain, J.-B. Vogt, T. Auger, and A. Gessi, Nucl. Instrum. Methods Phys. Res., Sect. A **562**, 698 (2006).

[26] Materion—PF-60 Beryllium High Purity Foil, https://materion.com/resource-center/product-data-and-related-literature/beryllium/beryllium-x-ray-material (2023), accessed on January 29, 2023.

[27] L. Bruno *et al.*, CNGS reference parameter list, CERN Technical Report No. CERN-AB-Note-2004-063, 2004, https://cds.cern.ch/record/790194.

[28] V. Kuksenko, K. Ammigan, B. Hartsell, C. Densham, P. Hurh, and S. Roberts, J. Nucl. Mater. **490**, 260 (2017).

[29] K. Ammigan and P. Hurh, Status and updates of the RaDIATE Collaboration R&D Program, Fermilab, Batavia, IL, FERMILAB, Technical Report No. FERMILAB-CONF-17-563-AD, 2017.

[30] P. Hurh, in *Proceedings of the North American Particle Accelerator Conference, NAPAC-2016, Chicago, IL* (JACoW, Geneva, Switzerland, 2017), p. 4.

[31] K. Ammigan, P. Hurh, and R. M. Zwaska, in *Proceedings of the 8th International Particle Accelerator Conference, IPAC-2018, Copenhagen, Denmark* (JACoW, Geneva, Switzerland, 2017), p. 4.

[32] N. Simos, H. Ludewig, H. Kirk, E. Dooryhee, S. Ghose, Z. Zhong, H. Zhong, S. Makimura, K. Yoshimura, J. R. J. Bennett, G. Kotsinas, Z. Kotsina, and K. T. McDonald, Phys. Rev. Accel. Beams **21**, 053001 (2018).

[33] K. Ammigan, A. Atherton, M. Butcher, M. Calviani, O. Caretta, T. Davenne, C. Densham, M. Fitton, M. Guinchard, B. Hartsell, P. Hurh, V. Kuksenko, R. Losito, P. Loveridge, J. O'Dell, S. Roberts, and R. Zwaska, in *Proceedings of the 6th International Particle Accelerator Conference, IPAC-2015, Richmond, VA* (JACoW, Geneva, Switzerland, 2015), p. 4.

[34] K. Ammigan, B. Hartsell, P. Hurh, R. Zwaska, M. Butcher, M. Guinchard, M. Calviani, R. Losito, S. Roberts, V. Kuksenko, A. Atherton, O. Caretta, T. Davenne, C. Densham, M. Fitton, J. Loveridge, and J. O'Dell, in *Proceedings of North American Particle Accelerator Conference, NAPAC-2016, Chicago, IL* (JACoW, Geneva, Switzerland, 2017), p. 4.

[35] K. Ammigan, S. Bidhar, P. Hurh, R. Zwaska, M. Butcher, M. Calviani, M. Guinchard, R. Losito, V. Kuksenko, S. Roberts, A. Atherton, G. Burton, O. Caretta, T. Davenne, C. Densham, M. Fitton, P. Loveridge, and J. O'Dell, Phys. Rev. Accel. Beams **22**, 044501 (2019).

[36] K. Ammigan and E. Lansing, in *Proceedings of the 2018 High Power Targetry Workshop* (FRIB Laboratory, East Lansing, Michigan, USA, 2018), https://indico.fnal.gov/event/15204/contributions/30219/.

[37] C. Pasquino, J. F. Somoza, A. Harrison, N. Charitonidis, P. Simon, F. Velotti, M. Calviani, N. Solieri, and F. Carra, HiRadMat Technical Board: HRM-59 Windows Experiment (SMAUG), CERN Technical Report, 2022.

[38] M. Monteil, Inventory of windows for CERN accelerators, CERN, Technical Report No. Document 1074871 (v.1), 2014.

[39] T. Ishida, C. J. Densham, M. Fitton, E. Harvey-Fishenden, and A. Atherthon, in *Proceedings of the Neutrino Beams and Instrumentation, (NBI-2019), Batavia, IL* (Fermilab, 2019), p. 25.

[40] T. Ishida, E. Wakai, S. Makimura, P. G. Hurh, K. Ammigan, A. M. Casella, D. J. Edwards, D. J. Senor, C. J. Densham, M. Fitton, J. Bennett, D. Kim, N. Simos, M. Calviani, and C. Torregrosa Martin, in *Proceedings of the 14th International Workshop on Spallation Materials Technology* (The Physical Society of Japan, Fukushima, Japan, 2020).

[41] T. Ishida, E. Wakai, S. Makimura, A. M. Casella, D. J. Edwards, R. Prabhakaran, D. J. Senor, K. Ammigan, S. Bidhar, P. G. Hurh, F. Pellemoine, C. J. Densham, M. D. Fitton, J. M. Bennett, D. Kim, N. Simos, M. Hagiwara, N. Kawamura, S.-i. Meigo, and K. Yonehara, J. Nucl. Mater. **541**, 152413 (2020).

[42] P. Marmy and T. Leguey, J. Nucl. Mater. **296**, 155 (2001).

[43] L. K. Mansur, Survey of radiation effects in titanium alloys, Oak Ridge National Laboratory Technical Report No. ORNL/TM-2008/137, 2008.

[44] T. Ishida *et al.*, Nucl. Mater. Energy **15**, 169 (2018).

[45] K. Ammigan *et al.*, Fermilab Technical Report No. FERMILAB-CONF-22-139-AD, 2022, https://www.osti.gov/biblio/1856219.

[46] J. Pinson, A window of opportunity: Physicists test titanium target windows for particle beam, https://news.fnal.gov/2020/05/a-window-of-opportunity-physicists-test-titanium-target-windows-for-particle-beam/ (2020), accessed on January 21, 2023.

[47] T. Byun and K. Farrell, J. Nucl. Mater. **318**, 292 (2003).

[48] C. D. Fincher, H. Turman, A. French, M. Chancey, J. Gigax, E. Aydogan, D. Zhao, D. Yadav, K. Xie, Y. Wang,

M. Borden, L. Shao, S. A. Maloy, and M. Pharr, Nucl. Instrum. Methods Phys. Res., Sect. B **479**, 157 (2020).
[49] E. M. O'Brien *et al.*, Nucl. Instrum. Methods Phys. Res., Sect. A **956**, 163316 (2020).
[50] D. A. McClintock, M. N. Gussev, C. Campbell, K. Mao, T. G. Lach, W. Lu, J. A. Hachtel, and K. A. Unocic, Acta Mater. **231**, 117889 (2022).
[51] M. James, S. Maloy, F. Gac, W. Sommer, J. Chen, and H. Ullmaier, J. Nucl. Mater. **296**, 139 (2001).
[52] H. T. Bach, O. Anderoglu, T. A. Saleh, T. J. Romero, C. T. Kelsey, E. R. Olivas, B. H. Sencer, P. O. Dickerson, M. A. Connors, K. D. John, and S. A. Maloy, J. Nucl. Mater. **459**, 103 (2015).
[53] S. A. Maloy, T. J. Romero, P. Hosemann, M. B. Toloczko, and Y. Dai, J. Nucl. Mater. **417**, 1005 (2011).
[54] C. Silva, M. Song, M. Wang, K. Holliday, K. Leonard, G. Was, and J. Busby, J. Nucl. Mater. **551**, 152954 (2021).
[55] H. R. Brager and F. A. Garner, J. Nucl. Mater. **108–109**, 347 (1982).
[56] K. Farrell and T. S. Byun, J. Nucl. Mater. **296**, 129 (2001).
[57] S. A. Maloy, M. R. James, G. Willcutt, W. F. Sommer, M. Sokolov, L. L. Snead, M. L. Hamilton, and F. Garner, J. Nucl. Mater. **296**, 119 (2001).
[58] L. K. Mansur and J. R. Haines, J. Nucl. Mater. **356**, 1 (2006).
[59] D. A. McClintock, M. N. Gussev, C. Campbell, and W. Lu, J. Nucl. Mater. **545**, 152729 (2021).
[60] A. Presland, D. Ramos, B. Goddard, J.-M. Jimenez, and R. Veness, in *Proceedings of the 2005 Particle Accelerator Conference, Knoxville, TN* (IEEE, New York, 2005), pp. 1698–1700.
[61] M. Brice and C. Marcelloni, One of the beam dump of the LHC machine at point 6 – CERN-AC-0807025-04, 2008, https://cds.cern.ch/record/1141513.
[62] G.Bregliozzi, in *10th LHC Operations "Evian" Workshop* (CERN, 2021), https://indico.cern.ch/event/1077835/contributions/4615043/.
[63] Y. Dai, G. S. Bauer, F. Carsughi, H. Ullmaier, S. A. Maloy, and W. F. Sommer, J. Nucl. Mater. **265**, 203 (1999).
[64] R. L. Klueh, K. Ehrlich, and F. Abe, J. Nucl. Mater. **191–194**, 116 (1992).
[65] Y. Dai, F. Carsughi, W. F. Sommer, G. S. Bauer, and H. Ullmaier, J. Nucl. Mater. **276**, 289 (2000).
[66] T. Sugawara, K. Nishihara, H. Obayashi, Y. Kurata, and H. Oigawa, J. Nucl. Sci. Technol. **47**, 953 (2010).
[67] L. Zanini *et al.*, J. Nucl. Mater. **415**, 367 (2011).
[68] T. Sugawara, Y. Eguchi, H. Obayashi, H. Iwamoto, and K. Tsujimoto, Nucl. Eng. Des. **331**, 11 (2018).
[69] Y. Dai, Final report on MEGAPIE target irradiation and post-irradiation examination, Paul Scherrer-Institut, Switzerland, Technical Report No. NE0000652, 2015.
[70] C. Fazio *et al.*, Nucl. Eng. Des. **238**, 1471 (2008).
[71] Y. Dai, J. Henry, T. Auger, J. B. Vogt, A. Almazouzi, H. Glasbrenner, and F. Groeschel, J. Nucl. Mater. **356**, 308 (2006).
[72] Technical design report on J-PARC Transmutation Experimental Facility; ADS Target Test Facility (TEF-T), JAEA-Technology 2017-003, J-PARC Nuclear Transmutation Division, Technical Report, 2017.
[73] T. Sasa, S. Saito, H. Obayashi, and G. Ariyoshi, JPS Conf. Proc. **33**, 011051 (2021).
[74] T. Sasa, in *Nuclear Back-end and Transmutation Technology for Waste Disposal: Beyond the Fukushima Accident*, edited by K. Nakajima (Springer, Japan, 2015), pp. 73–79.
[75] S. Sgobba, in *Proceedings of the 2017 CERN–Accelerator–School Course on Vacuum for Particle Accelerators, Glumslov, Sweden*, arXiv:2006.02212).
[76] Y. Dai and D. Hamaguchi, J. Nucl. Mater. **343**, 184 (2005).
[77] D. Blanco Lopez, in *Proceedings of the 2018 High Power Targetry Workshop* (2018), p. 21, https://indico.fnal.gov/event/15204/contributions/30159/attachments/18935/23730/21-An_engineering_review_of_ISIS_PBW.pdf.
[78] H. Takada, K. Haga, M. Teshigawara, T. Aso, S.-I. Meigo, H. Kogawa, T. Naoe, T. Wakui, M. Ooi, M. Harada, and M. Futakawa, Quantum Beam Sci. **1**, 8 (2017).
[79] T. Ibaraki, Technical design report of spallation neutron source facility in J-PARC, J-PARC Technical Report No. JAEA-Technology-2011-035, 2012.
[80] H.-J. Wang, W.-B. Liu, H.-M. Qu, D.-H. Zhu, N. Huang, L. Kang, and R.-H. Liu, Chin. Phys. C **37**, 077001 (2013).
[81] K. Farrell, J. Nucl. Mater. **97**, 33 (1981).
[82] D. Hamaguchi and Y. Dai, J. Nucl. Mater. **329–333**, 958 (2004).
[83] K. Farrell, Assessment of aluminum structural materials for service within the ANS reflector vessel, Oak Ridge National Laboratory, Technical Report No. ORNL/TM–13049, 1995.
[84] K. Farrell, Cold neutron source, Oak Ridge National Laboratory Technical Report No. ORNL/TM-1999/208, 1999.
[85] B. N. Singh, A. Horsewell, W. F. Sommer, and W. Lohmann, J. Nucl. Mater. **141–143**, 718 (1986).
[86] M. Butzek, J. Wolters, and B. Laatsch, in *Proceedings of the 4th High Power Targetry Workshop, Malmö, Sweden* (2011), p. 15, http://kirkmcd.princeton.edu/mumu/target/Butzek/Butzek_050211.pdf.
[87] R. Vivanco, T. Mora, J. Aguilar, M. Magán, I. Herranz, A. Aguilar, L. Mena, M. Mancisidor, G. Bakedano, P. Luna, F. Jiménez-Villacorta, M. Wilborgsson, F. Sordo, J. M. Perlado, and J. L. Martínez, J. Phys. Conf. Ser. **1021**, 012065 (2018).
[88] Y. Lee, J. Neutron Res. **22**, 299 (2020).
[89] D. Aulet, Y. Dai, R. M. Bergmann, and M. Wohlmuther, Nucl. Instrum. Methods Phys. Res., Sect. A **922**, 310 (2019).
[90] Y. Dai and W. Wagner, in *Proceedings of the International Topical Meeting on Nuclear Research Applications and Utilization of Accelerators, Vienna* (Paul Scherrer Institut, Switzerland, 2009), p. 28.
[91] D. L. Chung, MRS Bull. **44**, 661 (2019).
[92] Microstructure and physical properties of glassy carbon SIGRADUR, http://www.htw-germany.com/technology.php5?lang=en&nav0=2&nav1=0, accessed on January 27, 2023.

[93] Carbon Fiber-Reinforced Carbon—SGL Carbon Group, www.sglcarbon.com, accessed on January 29, 2023.
[94] N. Simos, H. Kirk, S. Kahn, K. McDonald, M. Cates, B. Riemer, J. Tsai, and D. Beshears, in *Proceedings of 8th European Particle Accelerator Conference, Paris, France*, edited by J.-L. Laclare (EPS-IGA and CERN, Geneva, Switzerland, 2002), Vol. 0206031, pp. 2709–2711.
[95] P. Simon, P. Drechsel, P. Katrik, K.-O. Voss, P. Bolz, F. J. Harden, M. Guinchard, Y. Kadi, C. Trautmann, and M. Tomut, Shock Vib. **2021**, 1 (2021).
[96] P. Andreu Muñoz, M. Calviani, N. Charitonidis, A. Cherif, E. Farina, A. Krainer, A. Lechner, J. Maestre, F.-X. Nuiry, R. Seidenbinder, P. Simon, and C. Torregrosa, in *Proceedings of the 13th International Particle Accelerator Conference, IPAC-2022* (JACoW, Geneva, Switzerland, 2022), p. 4.
[97] M. Pasquali, A. Bertarelli, C. Accettura, E. Berthome, L. Bianchi, P. Bolz, F. Carra, C. Fichera, M. Frankl, and T. Furness, J. Dyn. Behav. Mater. **5**, 266 (2019).
[98] L. dos Santos Conejo, H. R. de Meneses Neto, J. B. de Oliveira, L. F. de Paula Santos, R. Z. Nakazato, L. R. de Oliveira Hein, W. Kok, and E. C. Botelho, J. Polym. Res. **28**, 123 (2021).
[99] C. Garion, World J. Mech. **4**, 79 (2014).
[100] L. Baudin, Glassy carbon experiment in the HiRadMat Facility—Engineering note. glassy carbon window. Thermomechanical studies, CERN Technical Report No. 1751949 (v.1), 2017.
[101] L. Baudin, Glassy carbon experiment in the HiRadMat Facility—Engineering note. Glassy carbon window. Vacuum performance studies, CERN Technical Report No. 1751949 (v.1), 2017.
[102] P. Simon, S. Burger, N. Charitonidis, and C. Pasquino, Glassy carbon beam windows at HiRadMat, CERN Technical Report, 2021.
[103] V.-P. Viitanen, R. Mutikainen, S. Nenonen, and P. Partanen, J. X-Ray Sci. Technol. **4**, 182 (1994).
[104] P. T. Törmä, H. J. Sipilä, M. Mattila, P. Kostamo, J. Kostamo, E. Kostamo, H. Lipsanen, N. Nelms, B. Shortt, M. Bavdaz, and C. Laubis, IEEE Trans. Nucl. Sci. **60**, 1311 (2013).
[105] Silson—Silicon nitride, https://www.silson.com/product/silicon-nitride/ (2023), accessed on January 31, 2023.
[106] Silson—Silicon carbide, https://www.silson.com/product/silicon-carbide/ (2023), accessed on January 31, 2023.
[107] S. Huebner, N. Miyakawa, S. Kapser, A. Pahlke, and F. Kreupl, IEEE Trans. Nucl. Sci. **62**, 588 (2015).
[108] H. Wang, H. Jing, H. Qu, and J. Tang, in *Proceedings of the 5th International Particle Accelerator Conference, IPAC-2014, Dresden, Germany* (JACoW, Geneva, Switzerland, 2014), p. 3.
[109] H. Wang, C. Meng, H. Qu, X. Sun, P. Wang, and D. Zhu, in *Proceedings of the 9th International Particle Accelerator Conference, IPAC-2018, Vancouver, BC, Canada* (JACoW, Geneva, Switzerland, 2018), p. 4.
[110] S. Purushothaman, H. Haba, E. Haettner, S. Ishikawa, K. Itahashi, S. Y. Matsumoto, Y. Miyake, A. Sakaue, R. Sekiya, Y. K. Tanaka, and M. Tomut, First test of graphenic carbon vacuum windows with heavy ions, RIKEN Technical Report No. 53, 2019.
[111] A. Bertarelli, in *Proceedings of the 2014 Joint International Accelerator School: Beam Loss and Accelerator Protection, Newport Beach, CA* (CERN, Geneva, Switzerland, 2016), Vol. 2, 10.5170/CERN-2016-002.159.